nature COMMUNICATIONS

ARTICLE

Received 11 Feb 2016 | Accepted 27 Jul 2016 | Published 28 Sep 2016

DOI: 10.1038/ncomms12774

OPEN

Robust upward dispersion of the neutron spin resonance in the heavy fermion superconductor $Ce_{1-x}Yb_xCoIn_5$

Yu Song[1], John Van Dyke[2], I.K. Lum[3,4,5], B.D. White[4,5], Sooyoung Jang[3,4,5], Duygu Yazici[3,4,5], L. Shu[6,7], A. Schneidewind[8], Petr Čermák[8], Y. Qiu[9], M.B. Maple[3,4,5], Dirk K. Morr[2] & Pengcheng Dai[1]

The neutron spin resonance is a collective magnetic excitation that appears in the unconventional copper oxide, iron pnictide and heavy fermion superconductors. Although the resonance is commonly associated with a spin-exciton due to the $d(s^{\pm})$-wave symmetry of the superconducting order parameter, it has also been proposed to be a magnon-like excitation appearing in the superconducting state. Here we use inelastic neutron scattering to demonstrate that the resonance in the heavy fermion superconductor $Ce_{1-x}Yb_xCoIn_5$ with $x=0$, 0.05 and 0.3 has a ring-like upward dispersion that is robust against Yb-doping. By comparing our experimental data with a random phase approximation calculation using the electronic structure and the momentum dependence of the $d_{x^2-y^2}$-wave superconducting gap determined from scanning tunnelling microscopy (STM) for $CeCoIn_5$, we conclude that the robust upward-dispersing resonance mode in $Ce_{1-x}Yb_xCoIn_5$ is inconsistent with the downward dispersion predicted within the spin-exciton scenario.

[1] Department of Physics and Astronomy, Rice University, Houston, Texas 77005, USA. [2] Department of Physics, University of Illinois at Chicago, Chicago, Illinois 60607, USA. [3] Materials Science and Engineering Program, University of California, San Diego, La Jolla, California 92093, USA. [4] Department of Physics, University of California, San Diego, La Jolla, California 92093, USA. [5] Center for Advanced Nanoscience, University of California, San Diego, La Jolla, California 92093, USA. [6] State Key Laboratory of Surface Physics, Department of Physics, Fudan University, Shanghai 200433, China. [7] Collaborative Innovation Center of Advanced Microstructures, Nanjing 210093, China. [8] Jülich Center for Neutron Science JCNS, Forschungszentrum Jülich GmbH, Outstation at MLZ, D-85747 Garching, Germany. [9] NIST Center for Neutron Research, National Institute of Standard and Technology, Gaithersburg, Maryland 20899, USA. Correspondence and requests for materials should be addressed to D.K.M. (email: dkmorr@uic.edu) or to P.D. (email: pdai@rice.edu).

Understanding the origin of unconventional superconductivity in strongly correlated electron materials continues to be at the forefront of modern condensed matter physics[1–5]. In copper oxide[6–8], iron pnictide[9,10] and heavy fermion[11,12] superconductors, the appearance of a neutron spin resonance below the superconducting transition temperature T_c suggests that spin-fluctuation-mediated pairing is a common thread for different families of unconventional superconductors[2].

The neutron spin resonance is a collective magnetic excitation coupled to superconductivity with a temperature dependence similar to the superconducting order parameter[6,7]. It is located near the antiferromagnetic (AF) ordering wave vector $\mathbf{Q}_{AF}$ of the undoped parent compound and its energy E_r at $\mathbf{Q}_{AF}$ is related to either T_c (ref. 13) or the superconducting energy gap Δ (ref. 14). Although it is generally accepted that the resonance is a signature of unconventional superconductivity[2], there is no consensus on its microscopic origin. A common interpretation of the resonance is that it is a spin-exciton, arising from particle-hole excitations involving momentum states near the Fermi surfaces that possess opposite signs of the d (or $s^{\pm}$)-wave superconducting order parameter[7,12,15]. Alternatively, it has also been proposed to be a magnon-like excitation[16,17]. At present, there is no consensus on its microscopic origin[2,7,8,10].

In hole-doped copper oxide superconductors, the magnetic excitations have an hourglass dispersion with a downward dispersion at energies below E_r and an upward magnon-like dispersion at energies above E_r (ref. 8). The resonance, on the other hand, obtained by subtracting the normal-state magnetic excitations from those in the superconducting state, displays predominantly a downward dispersion[18–21]. In the case of Ni-underdoped $BaFe_2As_2$ with coexisting AF order and superconductivity[22], the resonance only reveals an upward magnon-like dispersion[23]. In both cases, the resonance is well described by the spin-exciton scenario, the opposite dispersions being a result of $d_{x^2-y^2}$ or $s^{\pm}$ symmetry of the superconducting order parameter[23,24].

For the heavy fermion superconductor $CeCoIn_5$ ($T_c = 2.3$ K) (ref. 4), the resonance appears below T_c at $E_r = 0.60 \pm 0.03$ meV and the commensurate AF wave vector $\mathbf{Q}_{AF} = (1/2, 1/2, 1/2)$ in reciprocal space[12]. Since $CeCoIn_5$ has a superconducting gap with $d_{x^2-y^2}$-wave symmetry as determined from scanning tunnelling microscopy (STM) experiments[25,26], the resonance is expected to show a downward dispersion similar to the cuprates within the spin-exciton picture[27,28]. Alternatively, the resonance, with its three-dimensional character[12], could be a magnon-like excitation of f electrons that becomes visible due to its reduced decay rate in the superconducting state[16,17]. In this case, the resonance is not a signature of $d_{x^2-y^2}$-wave superconductivity, but a measure of the hybridization between f electrons and conduction electrons and its associated pairing-sensitive Landau damping[17].

When La is substituted for Ce in $Ce_{1-x}La_xCoIn_5$ (refs 29,30), superconductivity and the energy of the resonance are both rapidly suppressed, while E_r/k_BT_c remains approximately constant, where k_B is the Boltzmann constant. At the same time, the energy width of the resonance broadens with increasing La-doping[31,32]. When Yb is doped into $CeCoIn_5$ to form $Ce_{1-x}Yb_xCoIn_5$, superconductivity is suppressed much slower[33]. With increasing Yb, de Haas-van Alphen and angle-resolved photo-emission spectroscopy studies find a change in the Fermi-surface topology between Yb nominal doping levels of $x = 0.1$ and 0.2 (refs 34,35). In addition, London penetration depth measurements suggest that the superconducting gap changes from nodal to nodeless around a similar Yb-doping level[36], arising possibly from composite electron pairing in a fully gapped superconductor for $x > 0.2$ (ref. 37). If the resonance in $CeCoIn_5$ is a spin-exciton, it should be dramatically affected by the Yb-doping-induced changes in Fermi surface topology and superconducting gap. On the other hand, if the resonance is a magnon-like excitation, it should be much less sensitive to Yb-doping across $x = 0.2$ and display a upward dispersion similar to spin waves in antiferromagnetically ordered nonsuperconducting $CeRhIn_5$ characteristic of a robust effective nearest-neighbour exchange coupling, regardless of its itinerant electron or local moment origin[7,38,39].

Here we use inelastic neutron scattering to demonstrate that the resonance in the heavy fermion superconductor $Ce_{1-x}Yb_xCoIn_5$ with $x = 0$, 0.05 and 0.3, and $T_c \approx 2.3$, 2.25 and 1.5 K, respectively (Methods section and Supplementary Fig. 1)[4,12,33], has a dominant ring-like upward dispersion that is robust against Yb-doping and the concomitant changes in electronic structure, a feature not present in the spin-exciton scenario. Moreover, a downward dispersion expected in the spin-exciton scenario is not observed. The robust upward dispersion of the resonance suggests that it may have a magnon-like contribution[17]. Specifically, we find that the resonance in $Ce_{0.95}Yb_{0.05}CoIn_5$ displays an upward dispersion along [H, H, 0.5], [0.5, K, 0.5] and [0.5, 0.5, L] as shown in Fig. 1d–f, respectively. Upon increasing Yb-doping to $x = 0.3$, the energy of the resonance at $\mathbf{Q}_{AF}$ decreases corresponding to the reduction in T_c (Supplementary Fig. 2), but the overall dispersion and location of the mode in reciprocal space remain unchanged. Upward dispersions similar to $Ce_{0.95}Yb_{0.05}CoIn_5$ are also found in undoped $CeCoIn_5$ and $Ce_{0.7}Yb_{0.3}CoIn_5$ (Supplementary Figs 3–5). Using the electronic structure and the momentum dependence of the $d_{x^2-y^2}$-wave superconducting gap determined from STM for $CeCoIn_5$ (Fig. 1g)[28], we calculate the feedback of superconductivity on the magnetic excitations within the spin-exciton scenario (Supplementary Note 1, Supplementary Figs 6–8). The resulting wave vector dependence of the spin-exciton along [0.5, K] and [H, H], which are shown in Fig. 1h,i, respectively, are inconsistent with the experimentally determined upward dispersion (solid lines). Similar dispersive resonances in $CeCoIn_5$ and $Ce_{0.7}Yb_{0.3}CoIn_5$ (Fig. 3, Supplementary Figs 3 and 4 and Fig. 5) are seen in spite of possible changes in the Fermi surface and superconducting gap symmetry on moving from $x = 0$ to 0.3 (refs 34–36), also inconsistent with the expectation that a spin-exciton should depend sensitively on the Fermi surface. We thus conclude that the upward-dispersing resonance mode in $Ce_{0.95}Yb_{0.05}CoIn_5$ cannot be interpreted as a spin-exciton arising from the feedback of unconventional d-wave superconductivity[12,27,28]. On the other hand, the similarity of the resonance's dispersion along the [H, H, 0.5] direction with the spin-wave dispersion in AF-ordered nonsuperconducting $CeRhIn_5$ along the same direction[38,39] (Fig. 1j) suggests that the upward-dispersing resonance may be magnon-like. In this scenario, the magnetic resonance arises since the opening of the superconducting gap leads to a strong suppression of Landau damping for preexisting magnon-like excitations, as shown in Fig. 1k,l (Supplementary Note 2 and Supplementary Figs 9–11). This is, therefore, the first experimental observation of a magnetic resonance in an unconventional superconductor that cannot be interpreted as a spin-exciton.

Results

Dispersion of the resonance in $Ce_{0.95}Yb_{0.05}CoIn_5$ along [H, H, 0.5] and [0.5, 0.5, L]. Using a tetragonal unit cell with $a = b = 4.60$ Å and $c = 7.51$ Å for $Ce_{0.95}Yb_{0.05}CoIn_5$ (Fig. 1a), we define the momentum transfer $\mathbf{Q}$ in three-dimensional reciprocal space in Å^{-1} as $\mathbf{Q} = H\mathbf{a}^* + K\mathbf{b}^* + L\mathbf{c}^*$, where H, K and L are Miller indices and $\mathbf{a}^* = \hat{\mathbf{a}}2\pi/a$, $\mathbf{b}^* = \hat{\mathbf{b}}2\pi/b$ and $\mathbf{c}^* = \hat{\mathbf{c}}2\pi/c$. The experiments are carried out using the [H, H, L] and [H, K, H]

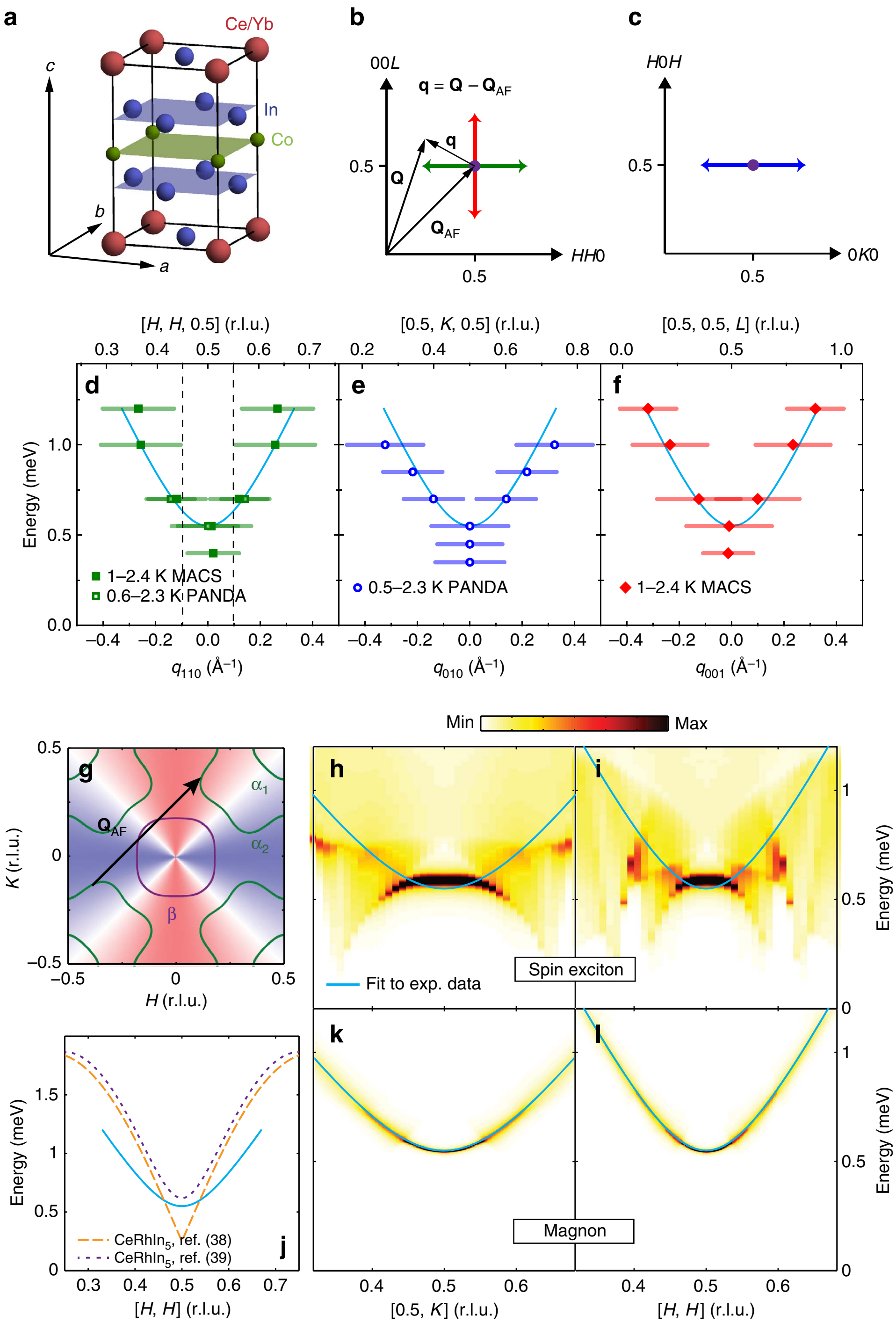

Figure 1 | Summary of neutron scattering results on $Ce_{0.95}Yb_{0.05}CoIn_5$. (**a**) Crystal structure of $Ce_{1-x}Yb_xCoIn_5$. (**b**) [*H*, *H*, *L*] scattering plane, where **q** is measured from $\mathbf{Q}_{AF}$ via $\mathbf{q}=\mathbf{Q}-\mathbf{Q}_{AF}$. The red and green arrows represent scans along [0.5, 0.5, *L*] and [*H*, *H*, 0.5] centred at $\mathbf{Q}_{AF}$, respectively. (**c**) [*H*, *K*, *H*] scattering plane. Here scans along [0.5, *K*, 0.5] centred at $\mathbf{Q}_{AF}$ can be carried out as indicated by the blue arrow. (**d**) Dispersion of the resonance along [*H*, *H*, 0.5]. The axis above the figure is **Q** in r.l.u., whereas the axis at the bottom is **q** in $Å^{-1}$. An isotropic dispersion $E=\sqrt{\Delta^2+(c|\mathbf{q}|)^2}$ ($\Delta=0.55(1)$ meV, $c=3.2(1)$ meV·Å) is shown as a cyan solid line, where Δ represents a spin gap and c is the effective spin wave velocity. The horizontal bars represent experimentally observed peak full-width-at-half-maximum. The dashed vertical lines indicate the ordering wave vector of the so-called *Q* phase at $\mathbf{Q}=\mathbf{Q}_{AF}\pm(\delta,\delta,0)$ with $\delta=0.05$ (ref. 44). (**e**,**f**) are similar to (**d**), but are for dispersions along [0.5, *K*, 0.5] and [0.5, 0.5, *L*], respectively. (**g**) The Fermi surfaces of $CeCoIn_5$, where the blue and red shading represent the *d*-wave symmetry of the superconductivity order parameter. The black arrow indicates $\mathbf{Q}_{AF}$, which connects parts of Fermi surfaces with sign-reversed superconductivity-order parameters. (**h**) Colour-coded calculated intensity along the [0.5, *K*] direction by considering the resonance mode to be a spin-exciton. (**i**) Calculated intensity for the spin-exciton along the [*H*, *H*] direction. (**j**) Comparison of dispersions of the resonance in $Ce_{0.95}Yb_{0.05}CoIn_5$ (solid cyan line) and spin waves in $CeRhIn_5$ (dashed purple and orange lines)[38,39]. (**k**) Calculated intensity of the resonance along the [0.5, *K*] direction assuming it is a magnon-like excitation. Dispersion of the magnon-like excitations is obtained from fits to experimental data and the intensity is affected by damping due to the particle – hole continuum. (**l**) Calculated intensity for the magnon-like excitation along the [*H*, *H*] direction.

scattering planes to study the dispersions of the resonance along [*H*, *H*, 0.5], [0.5, *K*, 0.5] and [0.5, 0.5, *L*] (Fig. 1b,c). Figure 2a shows the colour-coded plot of the spin excitations at 0.6 K obtained from fits to the raw data at energies $E=0.3$, 0.55, 0.7, 0.85 and 1 meV along [*H*, *H*, 0.5] for $Ce_{0.95}Yb_{0.05}CoIn_5$ (Fig. 2c). Although the data show a weak commensurate peak at $E=0.3$ meV, we see a clear commensurate resonance at $E_r\approx0.55$ meV and upward-dispersing incommensurate peaks for energies $E=0.7$, 0.85 and 1 meV. Figure 2b shows constant-energy scans at $E=0.7$ meV below and above T_c. At $T=2.3$ K, we see a broad peak centred at the commensurate AF wave vector $\mathbf{Q}_{AF}$. Upon cooling to below T_c at $T=0.6$ K, the commensurate peak becomes two incommensurate peaks, which disperse outward with increasing energy (Fig. 2c). Figure 2d shows constant-**Q** scans at $\mathbf{Q}_{AF}$ for temperatures $T=0.6$, 1.5 and 2.3 K. Similar to previous work on pure $CeCoIn_5$ (ref. 12), the data reveal a clear resonance at $E_r\approx0.55$ meV below T_c, and no peak in the normal state above T_c.

To further illustrate the dispersive nature of the resonance, we show in Fig. 3 maps of scattering intensities in the [*H*, *H*, *L*] scattering plane of the spin excitations at different energies above and below T_c obtained on the multi-axis crystal spectrometer (MACS) for $Ce_{0.95}Yb_{0.05}CoIn_5$. In the probed reciprocal space, we see clear spin excitations around $\mathbf{Q}_{AF}$, which disperse outward with increasing energy. At an energy ($E=0.4$ meV) below the resonance, spin excitations are commensurate below (Fig. 3a) and above (Fig. 3b) T_c. The constant-energy cuts of the data along the [*H*, *H*, 0.5] direction confirm this conclusion (Fig. 3c). Figure 3d–f shows similar scans at $E=0.55$ meV and indicate that the scattering becomes broader in reciprocal space. Upon moving to $E=0.7$ meV (Fig. 3g–i), 1.0 meV (Fig. 3j–l) and 1.2 meV (Fig. 3m–o), we see clear ring-like scattering dispersing away from $\mathbf{Q}_{AF}$ with increasing energy in the superconducting state. The normal-state scattering is commensurate at all energies, and this is most clearly seen in the constant-energy cuts along the [*H*, *H*, 0.5] direction. Based on the difference of data at 2.1 and 1 K in Fig. 3, one can compose the dispersions of the resonance along the [*H*, *H*, 0.5] (Fig. 1d) and [0.5, 0.5, *L*] (Fig. 1f) directions. By plotting the dispersion in $Å^{-1}$ away from $\mathbf{Q}_{AF}$ (**q** as defined in Fig. 1b), we see that the resonance disperses almost isotropically along these two directions.

Dispersion of the resonance in $Ce_{0.95}Yb_{0.05}CoIn_5$ along [0.5, *K*, 0.5]. In cuprate superconductors such as $YBa_2Cu_3O_{6.5}$ (ref. 21), $YBa_2Cu_3O_{6.6}$ (ref. 40) and $La_{1.875}Ba_{0.125}CuO_4$ (ref. 41), spin

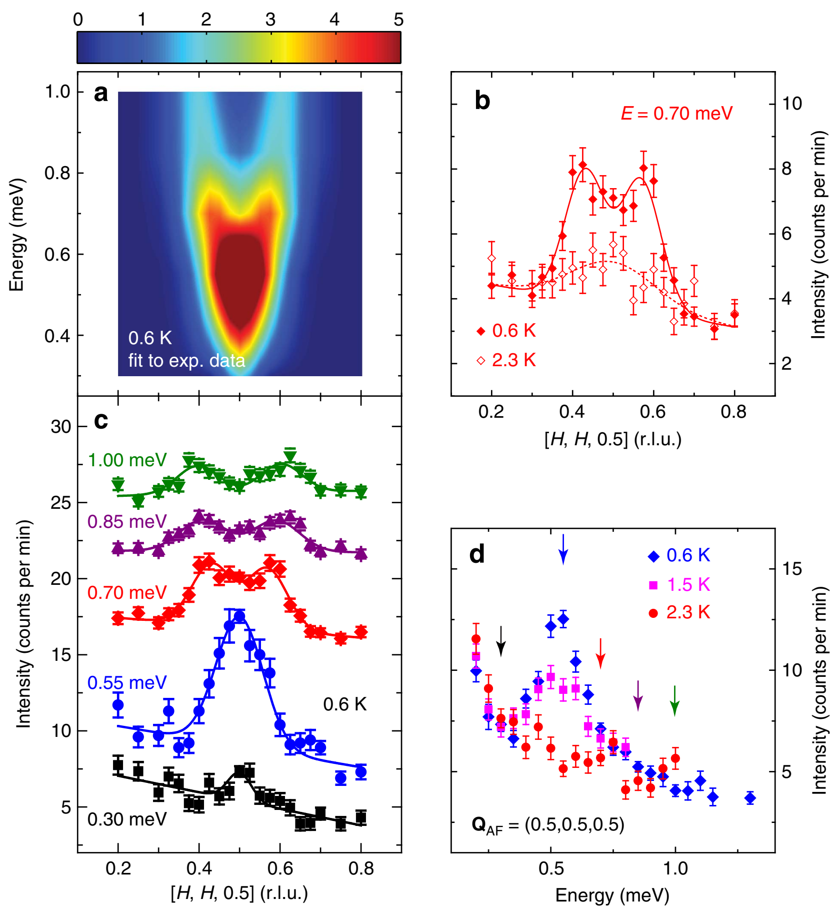

Figure 2 | Neutron scattering results on $Ce_{0.95}Yb_{0.05}CoIn_5$ in the [*H*, *H*, *L*] scattering plane. (**a**) Colour-coded intensity of magnetic excitations along [*H*, *H*, 0.5] centred at $\mathbf{Q}_{AF}$ at 0.6 K, obtained from fits to data in (**c**). (**b**) Constant-energy scans along [*H*, *H*, 0.5] centred at $\mathbf{Q}_{AF}$ with $E=0.7$ meV. The solid symbols are data well below T_c (0.6 K), where two peaks can be resolved whereas open symbols are obtained above T_c (2.3 K) showing a single peak centred at $\mathbf{Q}_{AF}$. The solid line is a fit to the data at 0.6 K with two Gaussian functions, whereas the dashed line is a fit to a single Gaussian function for the data at 2.3 K. Data at the two temperatures are fit simultaneously to have the same linear background. (**c**) Constant-energy scans along [*H*, *H*, 0.5] at 0.6 K. For clarity, scans with $E=0.55$, 0.75, 0.75 and 1 meV are, respectively, shifted upwards by 5, 13, 18 and 22. The solid lines are fits to either one or two Gaussian functions with a linear background. (**d**) Constant-**Q** scans at $\mathbf{Q}_{AF}$. The arrows represent energies for which constant-energy scans are shown in (**c**). All vertical error bars in the figure represent statistical errors of 1 s.d.

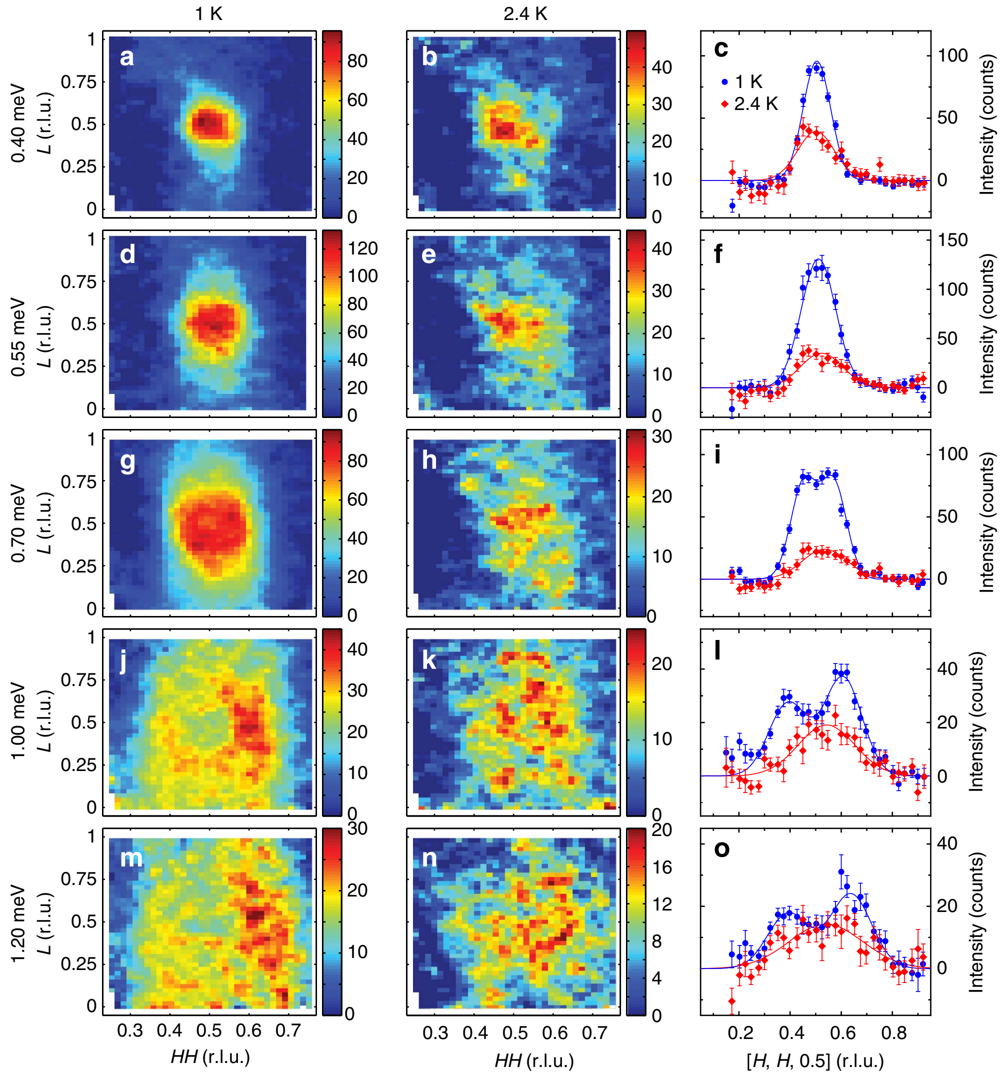

Figure 3 | Constant-energy maps of scattering intensities in the [*H*, *H*, *L*] scattering plane for $Ce_{0.95}Yb_{0.05}CoIn_5$. Constant-energy map at $E=0.40$ meV at (**a**) 1 K and (**b**) 2.4 K. A |**Q**|-dependent background has been subtracted. (**c**) Cuts obtained from (**a**,**b**) by binning data with $0.45\leq L\leq 0.55$; solid lines are fits to the data using either a single or two Gaussian functions. Since a background has already been subtracted in maps in (**a**,**b**), no background is assumed in the fits. Similarly, (**d**–**f**) are for $E=0.55$ meV, (**g**–**i**) are for $E=0.70$ meV, (**j**–**l**) are for $E=1.00$ meV and (**m**–**o**) are for $E=1.20$ meV. All vertical error bars in the figure represent statistical errors of 1 s.d.

excitations above the resonance form a ring-like upward dispersion in the *ab* plane slightly softened from the spin waves in their AF-ordered parent compounds[8]. To conclusively determine if the resonance dispersion is also ring-like in the *ab* plane in $Ce_{0.95}Yb_{0.05}CoIn_5$, we aligned the single crystals in the [*H*, 0, *H*] × [0, *K*, 0] ([*H*, *K*, *H*]) scattering plane to measure the dispersion of the resonance along [0.5, *K*, 0.5] centred at $\mathbf{Q}_{AF}$. Figure 4a–f summarizes the constant-energy scans at $E=0.35$, 0.45, 0.55, 0.7, 0.85 and 1.0 meV along [0.5, *K*, 0.5]. Although the scattering is clearly commensurate at $E=0.35$ and 0.45 meV below the resonance at $E_r\approx 0.55$ meV (Fig. 4a,b), it becomes incommensurate above the resonance at $E=0.7$, 0.85 and 1.0 meV with an upward dispersion as a function of increasing energy (Fig. 4d–f). Figure 1e summarizes the dispersion of the resonance in $Å^{-1}$ away from $\mathbf{Q}_{AF}$ along [0.5, *K*, 0.5]. Figure 4g shows the difference of the constant-**Q** scans below and above T_c at $\mathbf{Q}_{AF}$, again revealing a strong peak at the resonance energy of $E_r\approx 0.55$ meV similar to Fig. 2d. Finally, Fig. 4h shows the temperature dependence of the scattering at an incommensurate wave vector (0.5, 0.35, 0.5) and $E=0.85$ meV, which reveals a clear superconducting order-parameter-like increase below T_c and indicates that the incommensurate part of the resonance is also coupled to superconductivity.

Dispersion of the resonance for $CeCoIn_5$ and $Ce_{0.7}Yb_{0.3}CoIn_5$. To determine how Yb-doping, and in particular the possible changes in the Fermi surface topology and superconducting gap structure between Yb-doping of $x=0.1$ and 0.2, affects the behaviour of the resonance[34–36], we carried out additional inelastic neutron scattering experiments on $CeCoIn_5$ and $Ce_{0.7}Yb_{0.3}CoIn_5$ at MACS. Figure 5a shows temperature differences of constant-**Q** scans at $\mathbf{Q}_{AF}$ below and above T_c in $Ce_{0.7}Yb_{0.3}CoIn_5$, which reveals a clear resonance at $E_r\approx 0.4$ meV. Figure 5b plots the temperature dependence of the resonance, displaying a superconducting order-parameter-like increase in intensity below T_c. From wave vector scans along the [*H*, *H*, 0.5] and [0.5, 0.5, *L*] directions at different energies below and above T_c for $Ce_{0.7}Yb_{0.3}CoIn_5$ (Supplementary Fig. 5), we can establish the dispersions of the resonance along these two directions as shown in Fig. 5c,d, respectively. Similarly, Fig. 5e,f compares

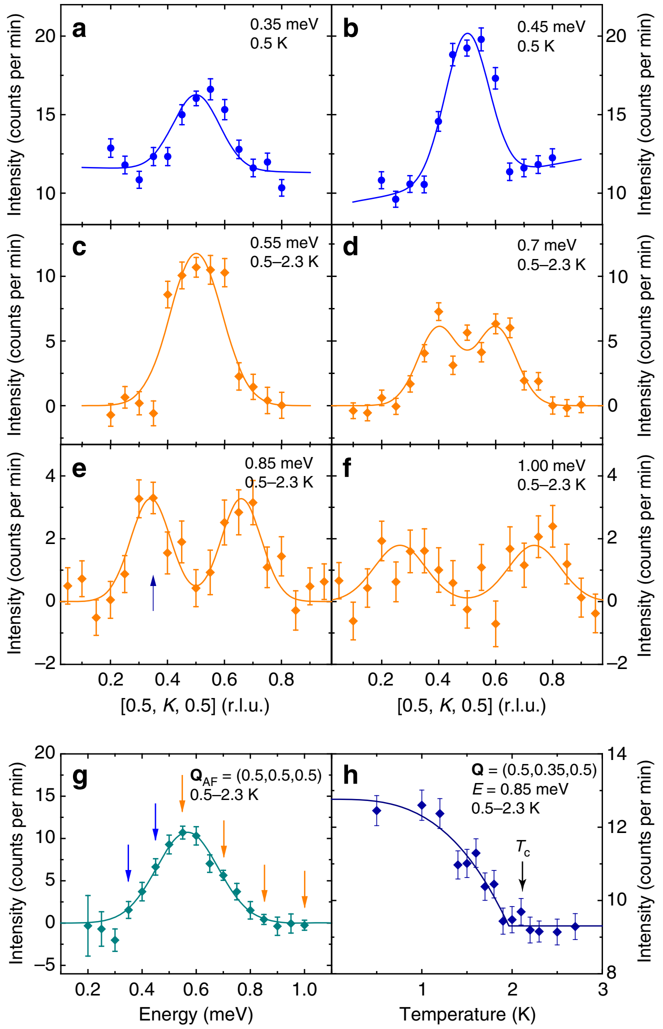

Figure 4 | Neutron scattering results on $Ce_{0.95}Yb_{0.05}CoIn_5$ in the [*H*, *K*, *H*] scattering plane. (**a**) Constant-energy scan along [0.5, *K*, 0.5] centred at $\mathbf{Q}_{AF}$ at 0.5 K for $E = 0.35$ meV. The solid line is a fit to a single Gaussian with a linear background. (**b**) Similar to (**a**), but for $E = 0.45$ meV. (**c**) Constant-energy scan along [0.5, *K*, 0.5] centred at $\mathbf{Q}_{AF}$, obtained by subtracting data at 2.3 K from data at 0.5 K for $E = 0.55$ meV. The solid line is a fit to a Gaussian function with zero background. (**d**) Similar to (**c**), but for $E = 0.7$ meV, and the solid line is a fit to two Gaussian functions. (**e**) Similar to (**d**), but for $E = 0.85$ meV. The arrow points to $\mathbf{Q} = (0.5, 0.35, 0.5)$, where measurement of the temperature dependence was carried out, shown in (**h**). (**f**) Similar to (**d**,**e**), but for $E = 1.00$ meV. (**g**) Constant-**Q** scan at $\mathbf{Q}_{AF}$ obtained by subtracting the 2.3 K data from the 0.5 K data. The solid line is a Gaussian function centred at $E = 0.57(1)$ meV with zero background. Arrows represent energies at which constant-energy scans are shown in (**a**–**f**). (**h**) Temperature dependence of scattering intensity at $\mathbf{Q} = (0.5, 0.35, 0.5)$ for $E = 0.85$ meV. The solid line is a fit to *d*-wave superconductivity order parameter with constant background. The superconducting critical temperature T_c obtained from the fit is 2.0(1) K. All vertical error bars in the figure represent statistical errors of 1 s.d.

dispersions of the resonance for $CeCoIn_5$ (Supplementary Fig. 4) and $Ce_{0.95}Yb_{0.05}CoIn_5$ along the [*H*, *H*, 0.5] and [0.5, 0.5, *L*] directions, respectively. From Fig. 5c–f, we see that the dispersions of the resonance are essentially Yb-doping independent. However, the bottom of the dispersive resonance at $\mathbf{Q}_{AF}$ moves down in energy with increasing Yb-doping and E_r is proportional to $k_B T_c$, similar to La-doped $CeCoIn_5$ (refs 31,32).

Discussion

From the dispersions of the resonance along [*H*, *H*, 0.5] (Fig. 1d), [0.5, *K*, 0.5] (Fig. 1e) and [0.5, 0.5, *L*] (Fig. 1f) for $Ce_{0.95}Yb_{0.05}CoIn_5$, we see that the mode disperses isotropically in reciprocal space away from $\mathbf{Q}_{AF}$, which is inconsistent with the resonance being a spin-exciton (see Fig. 1h,i), but resembles a magnon-like excitation with a dispersion similar to spin waves in $CeRhIn_5$ (Fig. 1j, Supplementary Note 3 and Supplementary Fig. 12) that becomes undamped in the superconducting state[16,17]. However, the fact that $CeCoIn_5$ is a multiband system complicates the identification of the resonance's origin. Athough we have assumed here that the main contribution to the resonance arises from the quasi-localized *f*-levels identified via quasi-particle interference (QPI) spectroscopy in STM experiment[25,28], it is of course possible that there exist further electronic bands that become superconducting and contribute to the resonance (either directly or through a renormalization of the magnetic interaction) but were not detected via QPI spectroscopy. Clearly, further studies are necessary to investigate this possibility.

Moreover, in a recent work on undoped $CeCoIn_5$, it was suggested that the resonance in the energy range of 0.4–0.7 meV is incommensurate along the [*H*, *H*, 0.5] direction with wave-vector $\mathbf{Q}_{AF} \pm (\delta, \delta, 0)$, where $\delta = 0.042(2)$ r.l.u. (ref. 42). Since the incommensurate wave vectors of the resonance appear to be close to the in-plane magnetic field-induced incommensurate static magnetic order at $\mathbf{Q}_{AF} \pm (\delta, \delta, 0)$ with $\delta = 0.05$ (the so-called *Q* phase) (see the vertical dashed lines in Fig. 1d)[43–45], and since it was suggested that the fluctuating moment of the resonance is entirely polarized along the *c*-axis similar to the ordered moment of the *Q* phase[12,42], the resonance has been described as a dynamical precursor of the *Q* phase[46]. Experimentally, we did not observe incommensurate excitations at $E = 0.5$ meV; nevertheless, our data suggest a smaller splitting than in previous work if the excitations at $E = 0.5$ are incommensurate (Supplementary Note 4 and Supplementary Fig. 13). Furthermore, the *Q* phase precursor interpretation of the resonance is also inconsistent with the observed ring-like dispersion at $E > 0.7$ meV. It is possible that there are more than one contribution to the resonance in $CeCoIn_5$ given its electronic complexity. In the present work, we identify the upward-dispersing magnon-like contribution as being dominant, but do not rule out finer features at lower energies with $E < 0.6$ meV, which can only be resolved with better resolution. Our data and previous work on $CeCoIn_5$ (ref. 42) are consistent with each other, both showing no signature of a downward dispersion.

Further insight into the nature of the resonance in $CeCoIn_5$ can be gained by considering its behaviour in an applied magnetic field. Previous neutron scattering experiments by Stock *et al.*[47] observed that the resonance in the superconducting state of $CeCoIn_5$ splits into two modes if a magnetic field is applied along the [1, $\bar{1}$, 0] direction. This splitting into two modes by an in-plane field is rather puzzling, since for a system with a Heisenberg spin symmetry a splitting into three modes is expected. Moreover, if the resonance in $CeCoIn_5$ was entirely polarized along the *c*-axis[12,42], application of an in-plane magnetic field should not split the resonance into the doublet observed experimentally[47,48]. However, this observation can be explained if the system possesses a magnetic anisotropy with a magnetic easy plane (indicated by the green ellipse in Fig. 6a) that is perpendicular to the direction of the applied magnetic field (red arrow in Fig. 6a). Since the magnetic field applied by Stock *et al.*[47] lies in the [1, $\bar{1}$, 0] direction, this implies that the easy plane is spanned by the unit vectors in the [0, 0, 1] and [1, 1, 0] directions. This leads us to suggest that the resonance in $CeCoIn_5$ should also have a component along the [1, 1, 0] direction in addition to the *c*-axis component similar to

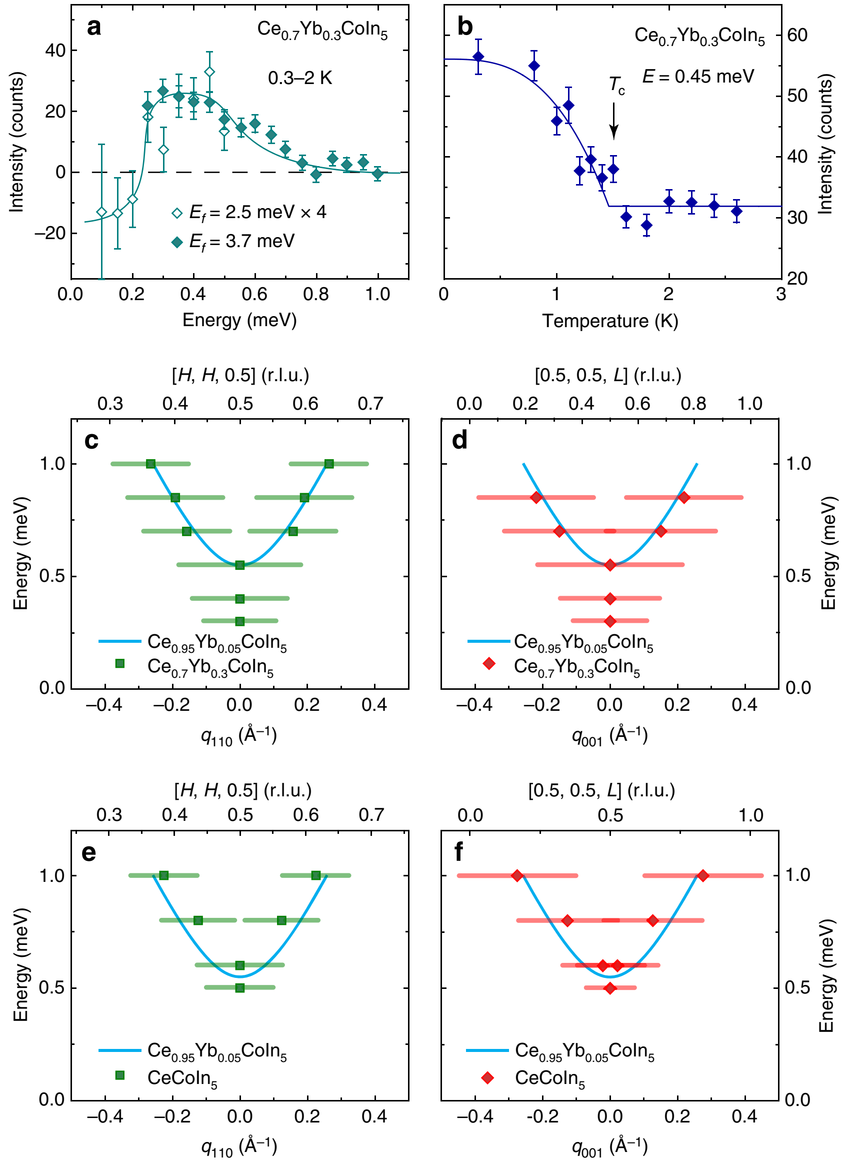

Figure 5 | Summary of neutron scattering results on $Ce_{0.7}Yb_{0.3}CoIn_5$ and $CeCoIn_5$. (**a**) Difference of constant-**Q** scans at $\mathbf{Q}_{AF} = (0.5, 0.5, 0.5)$ for 0.3 and 2 K, displaying a resonance mode at $E_r \approx 0.4$ meV for $Ce_{0.7}Yb_{0.3}CoIn_5$. Filled symbols are obtained with fixed scattered neutron energy $E_f = 3.7$ meV and open symbols are for $E_f = 2.5$ meV scaled up by 4 times. All of the data in the rest of figure are obtained with $E_f = 3.7$ meV. The solid line is a guide to the eye. (**b**) Temperature dependence of the resonance mode in $Ce_{0.7}Yb_{0.3}CoIn_5$ for $E = 0.45$ meV and $\mathbf{Q}_{AF} = (0.5, 0.5, 0.5)$; the solid line is a fit to *d*-wave superconducting gap, with $T_c = 1.5(1)$ K. Dispersion of the resonance along (**c**) [*H*, *H*, 0.5] and (**d**) [0.5,0.5,*L*] for $Ce_{0.7}Yb_{0.3}CoIn_5$. Dispersions of the resonance for $CeCoIn_5$ along [*H*, *H*, 0.5] and [0.5, 0.5, *L*] are showin in (**e**,**f**), respectively. The solid cyan lines in (**c**–**f**) are dispersions of the resonance obtained for $Ce_{0.95}Yb_{0.05}CoIn_5$. The horizontal bars represent experimentally observed peak full-width-at-half-maximum. All vertical error bars in the figure represent statistical errors of 1 s.d.

the resonance in electron-doped iron pnictides[49,50]. Such in-plane spin excitation anisotropy can occur due to the presence of spin-orbit coupling, and does not break the four-fold rotational symmetry of the underlying lattice[50]. The present experimental results do not rule out the presence of such a mode, although it is also challenging to experimentally confirm its presence (Supplementary Note 5 and Supplementary Figs 14 and 15).

To quantitatively understand the effect of a magnetic field on spin excitations, we consider the Hamiltonian (see Supplementary Eq. 1 in ref. 28)

$$H = \sum_{\mathbf{r},\mathbf{r}'} I_{\mathbf{r},\mathbf{r}'} S_{\mathbf{r}} \cdot S_{\mathbf{r}'} + A \sum_{\mathbf{r}} \left(S^z_{\mathbf{r}}\right)^2 - g\mu_B H \sum_{\mathbf{r}} S^z_{\mathbf{r}} \qquad (1)$$

with the three terms representing the magnetic interactions between the *f*-electron moments, the magnetic anisotropy of the system and the interaction with the external magnetic field, respectively. Here, we define the direction of the magnetic field along the $[1, \bar{1}, 0]$ direction as the *z*-axis in spin space. We assume $A > 0$, such that the system possesses a hard magnetic axis along $[1, \bar{1}, 0]$ and an easy plane (green ellipse in Fig. 6a) perpendicular to it. This Hamiltonian implies that the effective interaction for the longitudinal, non-spin-flip scattering mode (parallel to the applied field) is given by $I_{zz}(\mathbf{q}) = I_{\mathbf{q}} + A$, while the interaction for the transverse mode is given by $I_{\pm}(\mathbf{q}) = I_{\mathbf{q}}$, with $I_{\mathbf{q}}$ being the Fourier transform of $I_{\mathbf{r},\mathbf{r}'}$ in Equation (1). In the vicinity of the AF wave-vector $\mathbf{Q}_{AF}$, where $I_{\mathbf{Q}_{AF}} < 0$, we thus obtain $|I_{zz}(\mathbf{Q}_{AF})| < |I_{\pm}(\mathbf{Q}_{AF})|$ since $A > 0$ for an easy plane perpendicular to the $[1, \bar{1}, 0]$ direction. This implies that the effective interaction

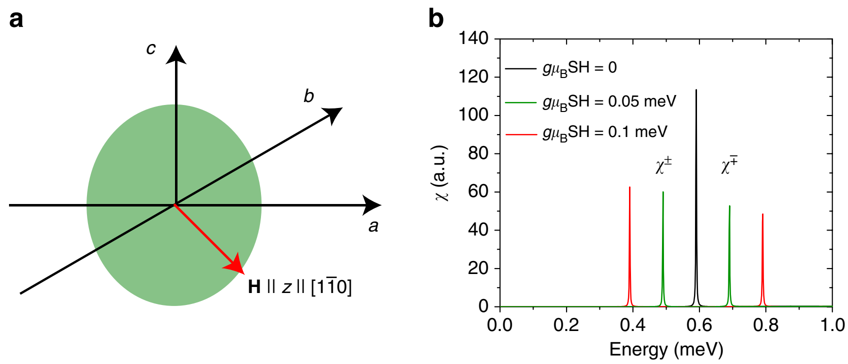

Figure 6 | Effect of applied magnetic field on the resonance mode. (**a**) Orientation of the magnetic field **H** and that of the magnetic easy plane in the crystal lattice. The magnetic field is perpendicular to the magnetic easy plane. (**b**) Evolution of the resonance with increasing magnetic field.

at $\mathbf{Q}_{AF}$ for the longitudinal, non-spin-flip scattering mode (parallel to the applied field) is smaller than for the two transverse, spin-flip scattering modes, which lie in the easy plane. As a result, the longitudinal mode will be located at energies higher than the transverse modes. In particular, for sufficiently large A, the longitudinal mode can be located above the onset energy, $\omega_c(\mathbf{Q}_{AF})$, for the particle–hole continuum in the superconducting state, and thus would not emerge as a resonance peak. Hence, only the two transverse modes within the easy plane contribute to the resonance peak. The application of a magnetic field perpendicular to the easy plane of the system then splits the two transverse modes of the resonance peak in energy (while not affecting the longitudinal mode), with the energy splitting increasing linearly with the magnetic field, as shown in Fig. 6b, thus explaining the experimental observation in ref. 47).

If spin excitations in $CeCoIn_5$ are only polarized along the c-axis with the existence of an easy axis rather than an easy plane[12,42], with application of a magnetic field along the direction perpendicular to the easy axis along the [1, $\bar{1}$, 0] direction, the transverse mode along the easy axis shifts down with increasing field, but does not split. Similarly, when a field is applied along the easy axis direction (c-axis field), the two transverse modes are located at higher energies, while the longitudinal mode, which is located at lower energies, does not split in the magnetic field. The presence of a longitudinal spin excitation along the [1, 1, 0] direction is also consistent with the magnetic field effect work of ref. 48, where the resonance is believed to be a composite excitation, which contains three excitation channels involving both transverse and longitudinal modes.

While unconventional superconductivity in copper oxide, iron pnictide and heavy fermion superconductors appears with the suppression of the static AF order in their parent compounds, dispersive magnon-like excitations persist in the doped superconductors[8,10,51]. Our discovery that the resonance itself in $Ce_{1-x}Yb_xCoIn_5$ shows a robust ring-like upwards dispersion suggests that, instead of being a spin-exciton in a d-wave superconductor[2,7], the resonance may be a magnon-like excitation revealed in the superconducting state[17]. Since the presence of a propagating spin resonance is characteristic of a nearby AF state, we propose that the magnon-like resonance mode in $Ce_{1-x}Yb_xCoIn_5$ is the strong-coupling analogue of a weak coupling spin-exciton. This would imply that the nature of the magnetic resonance—spin-exciton versus magnon-like excitation—represents a new criterion to distinguish between more weakly and more strongly coupled unconventional superconductors.

Methods

Sample preparation. Single crystals of $Ce_{1-x}Yb_xCoIn_5$ ($x = 0$, 0.05 and 0.3) were prepared by the indium self-flux method. Details of sample preparation and characterizations have been previously reported; lattice parameters for $Ce_{1-x}Yb_xCoIn_5$ remain similar to pure $CeCoIn_5$ for all reported doping levels[33]. We use the nominal doping throughout the paper to be consistent with earlier work[33], although the actual doping is $\sim 1/3$ of the nominal doping[52]. Supplementary Fig. 1a shows the out-of-phase AC magnetic susceptibility (15.9 Hz) measured on $Ce_{1-x}Yb_xCoIn_5$ samples with $x = 0.05$ and 0.3 from the same growth batches used for neutron scattering experiments. Bulk superconductivity appears at $T_c = 2.25$ K and $T_c = 1.5$ K, respectively, whereas $T_c = 2.3$ K in pure $CeCoIn_5$ (ref. 33).

Hundreds of $Ce_{1-x}Yb_xCoIn_5$ single crystals with total masses of 0.8, 2.5 and 1.4 g, respectively, for $x = 0$, 0.05 and 0.3 were co-aligned on several aluminium plates using CYTOP as hydrogen-free glue (Supplementary Fig. 1b). The plates are then mounted in either the [H, H, 0] × [0, 0, L] ([H, H, L]) (Supplementary Fig. 1c) or the [H, 0, H] × [0, K, 0] ([H, K, H]) scattering plane (Supplementary Fig. 1d). The total thickness of samples on co-aligned plates is 1–2 mm, minimizing neutron absorption due to indium. Absorption becomes most significant when the incident or the scattered neutron beam becomes perpendicular to [0, 0, 1], which does not occur for reciprocal space regions shown in this work.

Experiment details and analysis. Neutron scattering experiments were carried out on the PANDA cold triple-axes spectrometer[53] at Heinz Maier-Leibnitz Zentrum and the MACS instrument at the NIST Center for Neutron Research. The experiments on PANDA used a Be filter 180 mm in length after the sample, which is highly effective in removing contamination from higher-order neutrons; both the analyser and the monochromator are doubly focused to maximize neutron flux at the sample. Vertical focusing of the analyser is fixed, whereas horizontal focusing is variable. Both the horizontal and vertical focusing of the monochromator are variable. The variable focusings are adjusted depending on the neutron wavelength, which is based on empirically optimized values. The PANDA experiment in the [H, H, L] scattering plane used a fixed k_f of 1.3 $Å^{-1}$ ($E_f \approx 3.5$ meV) and the experiment in the [H, K, H] scattering plane used a fixed k_f of 1.57 $Å^{-1}$ ($E_f \approx 5.1$ meV). The MACS experiments in the [H, H, L] scattering plane used Be filters both before and after the sample with fixed $E_f = 3.7$ meV. MACS consists of 20 spectroscopic detectors, each separated by 8°. By rotating the sample and shifting all of the detectors to bridge the 8° gaps, a map in terms of sample rotation angle and scattering angle at a fixed energy transfer can be efficiently constructed. A significant portion of the reciprocal space in the scattering plane can be covered, which further allows cuts along the high-symmetry directions. Ninety-degree collimators are used between the sample and each individual analysers. The analysers are vertically focused, while the monochromator is doubly focused.

For the neutron scattering results on PANDA, a linear background is assumed for all measured constant-energy scans, while no background is used for scans obtained by subtracting data above T_c from those obtained below T_c. The constant-energy scans are then simply fit to either one or two Gaussian peaks. For the neutron scattering results obtained on MACS, maps of large portions of the scattering plane for several energy transfers were collected both below and above T_c. A $|\mathbf{Q}|$-dependent background is obtained by masking the signal near (0.5,0.5,0.5) and is then fit to a polynomial. The signal with $|\mathbf{Q}| < 0.5$ $Å^{-1}$ is masked throughout the analysis. The fit background is then subtracted from the map and the data are folded into the first quadrant of the scattering plane to improve statistics. The results for $Ce_{0.95}Yb_{0.05}CoIn_5$ are shown in Fig. 3 and Supplementary Fig. 3. Cuts along [H, H, 0.5] are obtained by binning data with $0.45 \leq L \leq 0.55$ and fit with a single or two Gaussian peaks. Cuts along [0.5, 0.5, L] are obtained by binning data with $0.45 \leq H \leq 0.55$ and fit by a sum of

Lorentzian peaks, accounting for the Ce^{3+} magnetic form factor $f(\mathbf{Q})$ and the polarization factor assuming excitations are dominantly polarized along the c-axis similar to previous work[12]. The possible presence of excitations polarized along the [1, 1, 0] direction is discussed in Supplementary Note 5. The function used to fit scans along [0.5, 0.5, L] can be written as

$$I(\mathbf{Q}) \propto f(\mathbf{Q})^2\left(1-\left(\hat{\mathbf{Q}}\cdot\hat{\mathbf{c}}\right)^2\right)\sum_{n=-\infty}^{\infty}F(n+L) \qquad (2)$$

where $F(L)$ is either a single Lorentizan peak centred at $L=0.5$ or two Lorentzian peaks equally displaced from $L=0.5$. The peaks along [0.5, 0.5, L] are significantly broader compared to those along [H, H, 0.5], and remain non-zero even for $L=0$ (Supplementary Fig. 3). This contrasts with similar scans along [H, H, 0.5] in Fig. 3, where the intensity drops to zero away from $\mathbf{Q}_{AF}$. MACS data of $CeCoIn_5$ and $Ce_{0.7}Yb_{0.3}CoIn_5$ with the corresponding maps and cuts are shown in Supplementary Figs 4 and 5. Similar to $Ce_{0.95}Yb_{0.05}CoIn_5$, the resonance mode clearly disperses upward with increasing energy.

Data availability. The data that support the findings of this study are available from the corresponding author upon request.

References

1. Monthoux, P., Pines, D. & Lonzarich, G. G. Superconductivity without phonons. *Nature* **450,** 1177–1183 (2007).
2. Scalapino, D. J. A common thread: the pairing interaction for unconventional superconductors. *Rev. Mod. Phys.* **84,** 1383 (2012).
3. Keimer, B., Kivelson, S. A., Norman, M. R., Uchida, S. & Zaanen, J. From quantum matter to high-temperature superconductivity in copper oxides. *Nature* **518,** 179–186 (2015).
4. Thompson, J. D. & Fisk, Z. Progress in heavy-fermion superconductivity: Ce115 and related materials. *J. Phys. Soc. Jpn* **81,** 011002 (2012).
5. White, B. D., Thompson, J. D. & Maple, M. B. Unconventional superconductivity in heavy-fermion compounds. *Physica C* **514,** 246–278 (2015).
6. Rossat-Mignod, J. *et al.* Neutron scattering study of the $YBa_2Cu_3O_{6+x}$ system. *Physica C* **185,** 86–92 (1991).
7. Eschrig, M. The effect of collective spin-1 excitations on electronic spectra in high-T_c superconductors. *Adv. Phys.* **55,** 47–183 (2006).
8. Tranquada, J. M., Xu, G. & Zaliznyak, I. A. Superconductivity, antiferromagnetism, and neutron scattering. *J. Mag. Mag. Mater* **350,** 148–160 (2014).
9. Christianson, A. D. *et al.* Resonant spin excitation in the high temperature superconductor $Ba_{0.6}K_{0.4}Fe_2As_2$. *Nature* **456,** 930–932 (2008).
10. Dai, P. C. Antiferromagnetic order and spin dynamics in iron-based superconductors. *Rev. Mod. Phys.* **87,** 855 (2015).
11. Sato, N. K. *et al.* Strong coupling between local moments and superconducting 'heavy' electrons in UPd_2Al_3. *Nature* **410,** 340–343 (2001).
12. Stock, C., Broholm, C., Hudis, J., Kang, H. J. & Petrovic, C. Spin resonance in the *d*-wave superconductor $CeCoIn_5$. *Phys. Rev. Lett.* **100,** 087001 (2008).
13. Inosov, D. S. *et al.* Crossover from weak to strong pairing in unconventional superconductors. *Phys. Rev. B* **83,** 214520 (2011).
14. Yu, G., Li, Y., Motoyama, E. M. & Greven, M. A universal relationship between magnetic resonance and superconducting gap in unconventional superconductors. *Nat. Phys.* **5,** 873–875 (2009).
15. Hirschfeld, P. J., Korshunov, M. M. & Mazin, I. I. Gap symmetry and structure of Fe-based superconductors. *Rep. Prog. Phys.* **74,** 124508 (2011).
16. Morr, D. K. & Pines, D. The resonance peak in cuprate superconductors. *Phys. Rev. Lett.* **81,** 1086 (1998).
17. Chubukov, A. V. & Gor'kov, L. P. Spin resonance in three-dimensional superconductors: the case of $CeCoIn_5$. *Phys. Rev. Lett.* **101,** 147004 (2008).
18. Bourges, P. *et al.* The spin excitation spectrum in superconducting $YBa_2Cu_3O_{6.85}$. *Science* **288,** 1234–1237 (2000).
19. Dai, P. C., Mook, H. A., Hunt, R. D. & Doğan, F. , Evolution of the resonance and incommensurate spin fluctuations in superconducting $YBa_2Cu_3O_{6+x}$. *Phys. Rev. B* **63,** 054525 (2001).
20. Reznik, D. *et al.* Dispersion of magnetic excitations in optimally doped superconductor $YBa_2Cu_3O_{6.95}$. *Phys. Rev. Lett.* **93,** 207003 (2004).
21. Stock, C. *et al.* From incommensurate to dispersive spin-fluctuations: the high-energy inelastic spectrum in superconducting $YBa_2Cu_3O_{6.5}$. *Phys. Rev. B* **71,** 024522 (2005).
22. Lu, X. Y. *et al.* Avoided quantum criticality and magnetoelastic coupling in $BaFe_{2-x}Ni_xAs_2$. *Phys. Rev. Lett.* **110,** 257001 (2013).
23. Kim, M. G. *et al.* Magnonlike dispersion of spin resonance in Ni-doped $BaFe_2As_2$. *Phys. Rev. Lett.* **110,** 177002 (2013).
24. Eremin, I., Morr, D. K., Chubukov, A. V., Bennemann, K. H. & Norman, M. R. Novel neutron resonance mode in $d_{x^2-y^2}$-wave superconductors. *Phys. Rev. Lett.* **94,** 147001 (2005).
25. Allan, M. P. *et al.* Imaging Cooper pairing of heavy fermions in $CeCoIn_5$. *Nat. Phys.* **9,** 468–473 (2013).
26. Zhou, B. B. *et al.* Visualizing nodal heavy fermion superconductivity in $CeCoIn_5$. *Nat. Phys.* **9,** 474–479 (2013).
27. Eremin, I., Zwicknagl, G., Thalmeier, P. & Fulde, P. Feedback spin resonance in superconducting $CeCu_2Si_2$ and $CeCoIn_5$. *Phys. Rev. Lett.* **101,** 187001 (2008).
28. Van Dyke, J. *et al.* Direct evidence for a magnetic f-electronmediated pairing mechanism of heavy-fermion superconductivity in $CeCoIn_5$. *PNAS* **111,** 11663–11667 (2014).
29. Petrovic, C., Bud'ko, S. L., Kogan, V. G. & Canfield, P. C. Effects of La substitution on the superconducting state of $CeCoIn_5$. *Phys. Rev. B* **66,** 054534 (2002).
30. Tanatar, M. A. *et al.* Unpaired electrons in the heavy-fermion superconductor $CeCoIn_5$. *Phys. Rev. Lett.* **95,** 067002 (2005).
31. Panarin, J., Raymond, S., Lapertot, G., Flouquet, J. & Mignot, J.-M. Effects of nonmagnetic La impurities on the spin resonance of $Ce_{1-x}La_xCoIn_5$ single crystals as seen via inelastic neutron scattering. *Phys. Rev. B* **84,** 052505 (2011).
32. Raymond, S., Panarin, S., Lapertot, G. & Flouquet, J. Evolution of the spin resonance of $CeCoIn_5$ as a function of magnetic field and La substitution. *J. Phys. Soc. Jpn* **80,** SB023 (2011).
33. Shu, L. *et al.* Correlated electron state in $Ce_{1-x}Yb_xCoIn_5$ stabilized by cooperative valence fluctuations. *Phys. Rev. Lett.* **106,** 156403 (2011).
34. Polyakov, A. *et al.* Fermi-surface evolution in Yb-substituted $CeCoIn_5$. *Phys. Rev. B* **85,** 245119 (2012).
35. Dudy, L. *et al.* Yb valence change in $Ce_{1-x}Yb_xCoIn_5$ from spectroscopy and bulk properties. *Phys. Rev. B* **88,** 165118 (2013).
36. Kim, H. *et al.* Nodal to nodeless superconducting energy-gap structure change concomitant with Fermi-surface reconstruction in the heavy-fermion compound $CeCoIn_5$. *Phys. Rev. Lett.* **114,** 027003 (2015).
37. Erten, O., Flint, R. & Coleman, P. Molecular pairing and fully gapped superconductivity in Yb-doped $CeCoIn_5$. *Phys. Rev. Lett.* **114,** 027002 (2015).
38. Das, P. *et al.* Magnitude of the magnetic exchange interaction in the heavy-fermion antiferromagnet $CeRhIn_5$. *Phys. Rev. Lett.* **113,** 246404 (2014).
39. Stock, C. *et al.* Single to multiquasiparticle excitations in the itinerant helical magnet $CeRhIn_5$. *Phys. Rev. Lett.* **114,** 247005 (2015).
40. Hayden, S. M., Mook, H. A., Dai, P. C., Perring, T. G. & Doğan, F. The structure of the high-energy spin excitations in a high-transition temperature superconductor. *Nature* **429,** 531–534 (2004).
41. Tranquada, J. M. *et al.* Quantum magnetic excitations from stripes in copper oxide superconductors. *Nature* **429,** 534–538 (2004).
42. Raymond, S. & Lapertot, G. Ising incommensurate spin resonance of $CeCoIn_5$: a dynamical precursor of the *Q* phase. *Phys. Rev. Lett.* **115,** 037001 (2015).
43. Kenzelmann, M. *et al.* Coupled superconducting and magnetic order in $CeCoIn_5$. *Science* **321,** 1652–1654 (2008).
44. Kenzelmann, M. *et al.* Evidence for a magnetically driven superconducting *Q* phase of $CeCoIn_5$. *Phys. Rev. Lett.* **104,** 127001 (2010).
45. Gerber, S. *et al.* Switching of magnetic domains reveals spatially inhomogeneous superconductivity. *Nat. Phys.* **10,** 126–129 (2014).
46. Michal, V. P. & Mineev, V. P. Field-induced spin-exciton condensation in the $d_{x^2-y^2}$-wave superconductor $CeCoIn_5$. *Phys. Rev. B* **84,** 052508 (2011).
47. Stock, C. *et al.* Magnetic field splitting of the spin resonance in $CeCoIn_5$. *Phys. Rev. Lett.* **109,** 167207 (2012).
48. Raymond, S., Kaneko, K., Hiess, A., Steffens, P. & Lapertot, G. Evidence for three fluctuation channels in the spin resonance of the unconventional superconductor $CeCoIn_5$. *Phys. Rev. Lett.* **109,** 237210 (2012).
49. Steffens, P. *et al.* Splitting of resonance excitations in nearly optimally doped $Ba(Fe_{0.94}Co_{0.06})_2As_2$: an inelastic neutron scattering study with polarization analysis. *Phys. Rev. Lett.* **110,** 137001 (2013).
50. Luo, H. Q. *et al.* Spin excitation anisotropy as a probe of orbital ordering in the paramagnetic tetragonal phase of superconducting $BaFe_{1.904}Ni_{0.096}As_2$. *Phys. Rev. Lett.* **111,** 107006 (2013).
51. Stockert, O. *et al.* Magnetically driven superconductivity in $CeCu_2Si_2$. *Nat. Phys.* **7,** 119–124 (2011).
52. Jang, S. *et al.* Resolution of the discrepancy between the variation of the physical properties of $Ce_{1-x}Yb_xCoIn_5$ single crystals and thin films with Yb composition. *Philos. Mag.* **94,** 4219–4231 (2014).
53. Heinz, Maier-Leibnitz Zentrum *et al.* PANDA: Cold three axes spectrometer. *J. Large-Scale Research Facilities* **1,** A12 (2015).

Acknowledgements

We thank Qimiao Si, S. Raymond and C. Stock for helpful discussions. We also thank S. Raymond for sharing with us his unpublished data on $CeCoIn_5$. We acknowledge help from Mengshu Liu, Xingye Lu and Wenliang Zhang for assistance with sample co-alignment, and Scott Carr, Weiyi Wang and Jose Rodriguez for preliminary measurements on $Ce_{0.7}Yb_{0.3}CoIn_5$. The neutron scattering work at Rice is supported by the U.S DOE, BES, under Grant No. DE-SC0012311 (P.D.). Part of the material characterization efforts at Rice is supported by the Robert A. Welch Foundation Grant No. C-1839 (P.D.). The research at UCSD was supported by the U.S. DOE, BES, under Grant No. DE-FG02-04ER46105 (sample synthesis), and the U.S. NSF, under Grant No. DMR-1206553 (sample characterization). The work by JVD and DKM was supported by the U.S. DOE, BES, under Grant No. DE-FG02-05ER46225. The research at National Institute of

Standards and Technology is in part supported by U.S. NSF, under Agreement No. DMR-1508249. The research at Fudan University is in part supported by the NSFC, under Grant No. 11474060.

Author contributions

The samples were prepared by I.K.L., B.D.W., S.J., D.Y., L.S. and M.B.M. Neutron scattering experiments were carried out by Y.S., A.S., P.C., Y.Q., and P.D. Data analysis was done by Y.S. Theoretical calculations were done by J.V. and D.K.M. The paper was written by P.D., D.K.M., and Y.S. with input from all co-authors.

Additional information

Supplementary Information accompanies this paper at http://www.nature.com/naturecommunications

Competing financial interests: The authors declare no competing financial interests.

How to cite this article: Song, Y. *et al.* Robust upward dispersion of the neutron spin resonance in the heavy fermion superconductor $Ce_{1-x}Yb_xCoIn_5$. *Nat. Commun.* 7:12774 doi: 10.1038/ncomms12774 (2016).

Supplementary Information:

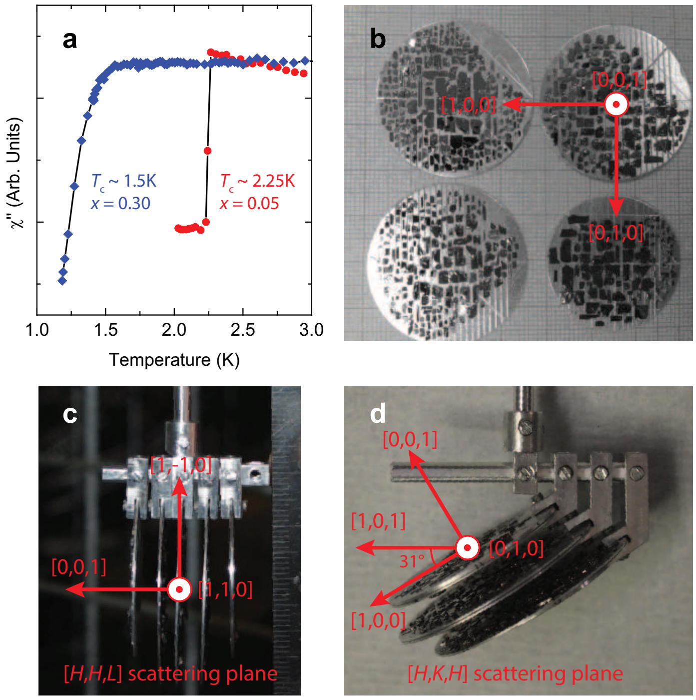

Supplementary Figure 1: Measurement of T_c and co-alignment of $Ce_{1-x}Yb_xCoIn_5$ single crystals. (a) AC magnetic susceptibility measured on $Ce_{1-x}Yb_xCoIn_5$ ($x = 0.05$ and 0.3), with T_c =2.25 K and 1.5 K. (b) Several aluminum plates with hundreds of co-aligned $Ce_{1-x}Yb_xCoIn_5$ ($x = 0.05$) single crystals. The crystallographic axes are marked by red arrows. (c) Co-aligned plates in the $[H, H, L]$ scattering plane. (d) Co-aligned plates in the $[H, K, H]$ scattering plane. The angle between $[1, 0, 1]$ and $[1, 0, 0]$ is $\sim 31^\circ$.

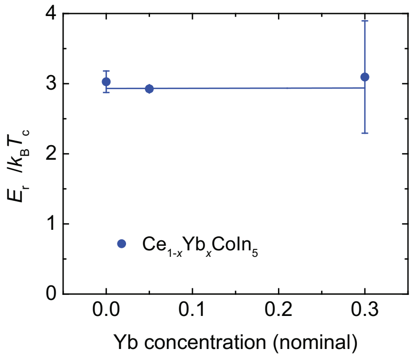

Supplementary Figure 2: $E_r/k_B T_c$ in $Ce_{1-x}Yb_xCoIn_5$. The result for $CeCoIn_5$ is obtained from previous work [1] and the results for $x = 0.05$ and $x = 0.3$ are from this work. The vertical error bars are estimates of the uncertainty of E_r by carrying out constant-$\mathbf{Q}$ scans at $\mathbf{Q}_{AF} = (0.5, 0.5, 0.5)$.

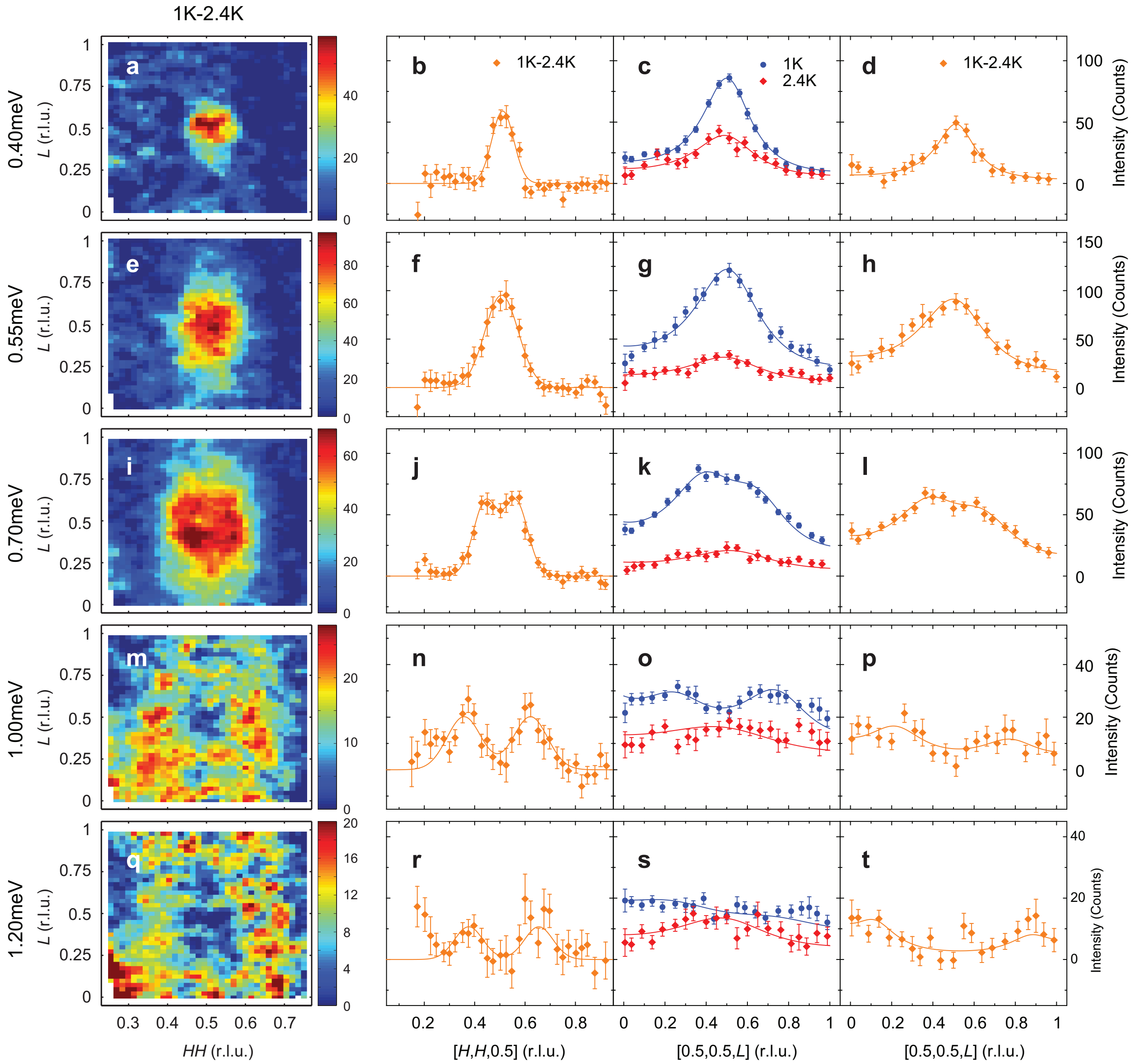

Supplementary Figure 3: Additional neutron scattering data for $Ce_{0.95}Yb_{0.05}CoIn_5$. (a) Constant-energy map for $Ce_{0.95}Yb_{0.05}CoIn_5$ at $E = 0.4$ meV and 1 K after subtracting data from 2.4 K. (b) Cut along $[H, H, 0.5]$ for the map in (a) at $E = 0.4$ meV, the solid line is a fit assuming zero background. (c) Cuts along $[0.5, 0.5, L]$ at both 1 K and 2.4 K obtained from maps in Figure 3(a) and (b) in the main text. (d) Cut along $[0.5, 0.5, L]$ for the map in (a) at 1K after subtracting data from 2.4 K. The solid lines in (c) and (d) are sums of Lorentzian peaks polarized along $\hat{\mathbf{c}}$. Similarly (e), (f), (g) and (h) are for $E = 0.55$ meV, (i), (j), (k) and (l) are for $E = 0.7$ meV, (m), (n), (o) and (p) are for $E = 1.00$ meV and (q), (r), (s) and (t) are for $E = 1.20$ meV. For cuts along $[0.5, 0.5, L]$ at 2.3 K and $E = 0.40$ and 0.55 meV, $F(L)$ is a single Lorentzian peak centered at $L = 0.5$. For 1 K and 1 K-2.4 K cuts with $E = 0.7, 1.0$ and 1.20 meV, $F(L)$ is two Lorentzian peaks equally displaced from $L = 0.5$. All vertical error bars in the Figure represent statistical errors of 1 standard deviation.

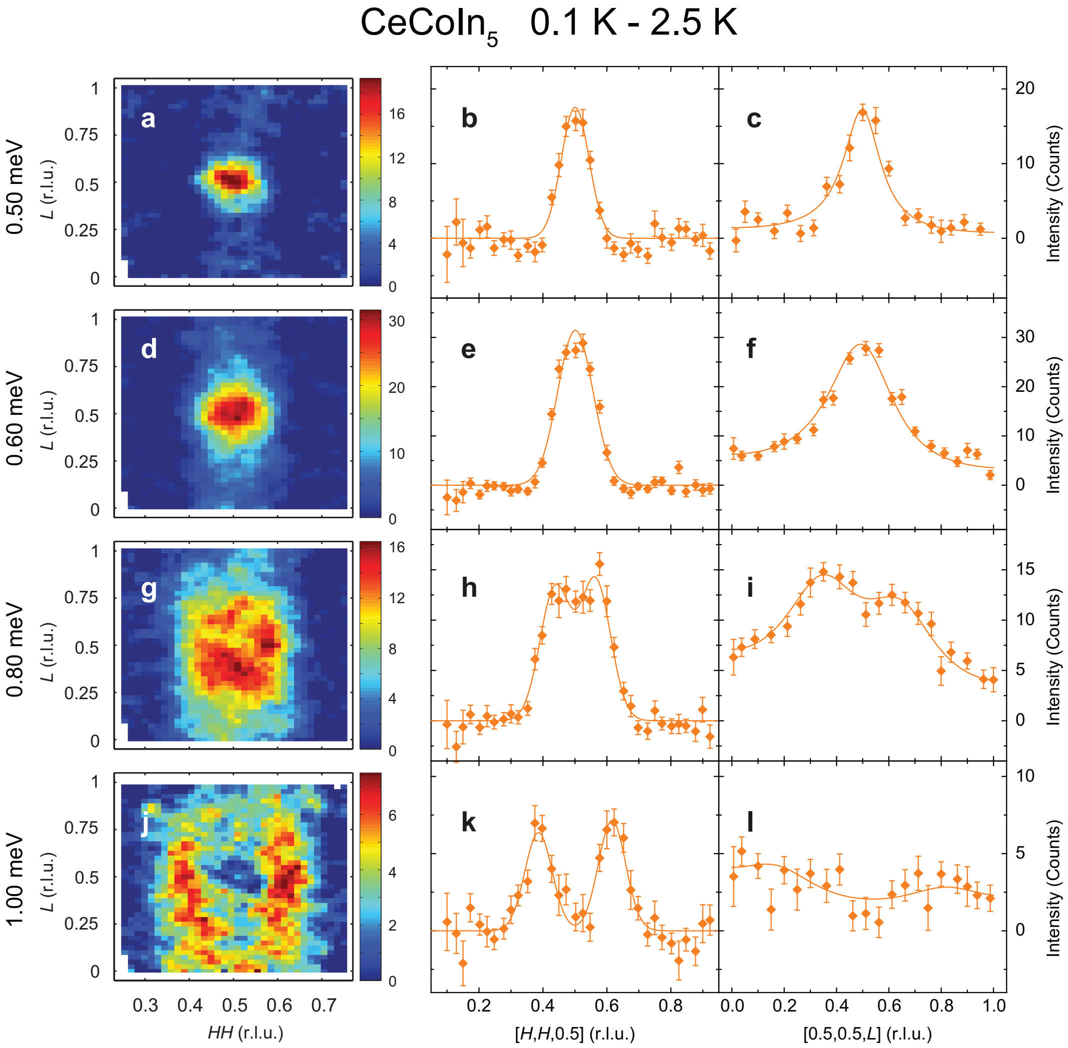

Supplementary Figure 4: Neutron scattering data for $CeCoIn_5$. (a) Constant-energy map for $CeCoIn_5$ at $E = 0.5$ meV and 0.1 K after subtracting data from 2.5 K. (b) Cut along $[H, H, 0.5]$ for the map in (a), the solid line is a fit assuming zero background. (c) Cut along $[0.5, 0.5, L]$ for the map in (a), the solid line is a sum of Lorentzian peaks polarized along $\hat{\mathbf{c}}$. Similarly (d), (e) and (f)are for $E = 0.6$ meV, (g), (h) and (i) are for $E = 0.8$ meV and (j), (k) and (l) are for $E = 1.00$ meV. For cuts along $[0.5, 0.5, L]$ for $E = 0.50$ and 0.60 meV, $F(L)$ is a single Lorentzian peak centered at $L = 0.5$. For $E = 0.8$ and 1.0 meV, $F(L)$ is two Lorentzian peaks equally displaced from $L = 0.5$. All vertical error bars in the Figure represent statistical errors of 1 standard deviation.

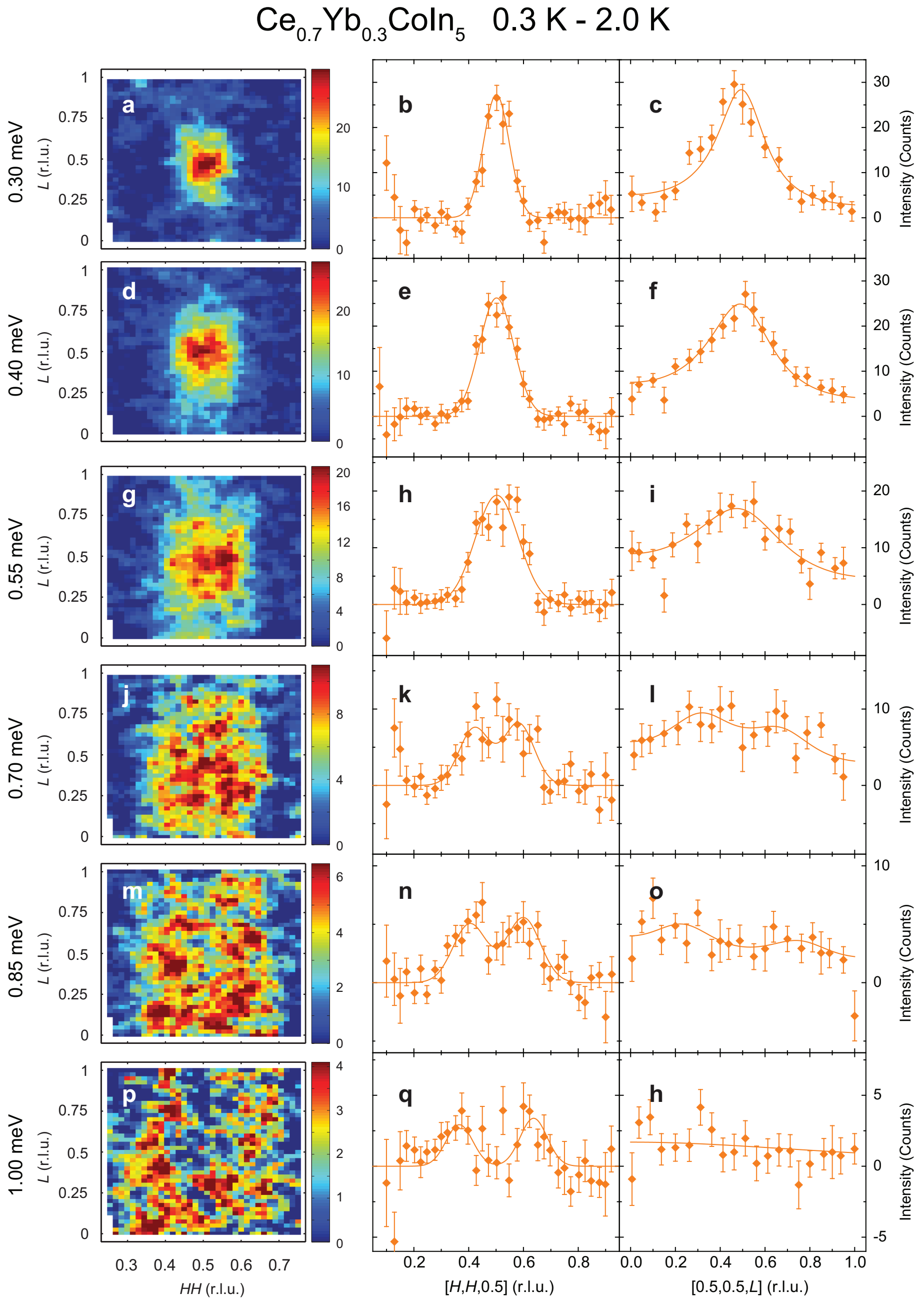

Supplementary Figure 5: Neutron scattering data for $Ce_{0.7}Yb_{0.3}CoIn_5$. (a) Constant-energy map for $Ce_{0.7}Yb_{0.3}CoIn_5$ at $E = 0.3$ meV and 0.3 K after subtracting data from 2.0 K. (b) Cut along $[H, H, 0.5]$ for the map in (a), the solid line is a fit assuming zero background. (c) Cut along $[0.5, 0.5, L]$ for the map in (a), the solid line is a sum of Lorentzian peaks polarized along $\hat{\mathbf{c}}$. Similarly (d), (e) and (f)are for $E = 0.4$ meV, (g), (h) and (i) are for $E = 0.55$ meV, (j), (k) and (l) are for $E = 0.7$ meV, (m), (n) and (o) are for $E = 0.85$ meV and (p), (q) and (r) are for $E = 1.0$ meV. For cuts along $[0.5, 0.5, L]$ for $E = 0.3$, 0.4 and 0.55 meV, $F(L)$ is a single Lorentzian peak centered at $L = 0.5$. For $E = 0.7$, 0.85 and 1.0 meV, $F(L)$ is two Lorentzian peaks equally displaced from $L = 0.5$. All vertical error bars in the Figure represent statistical errors of 1 standard deviation.

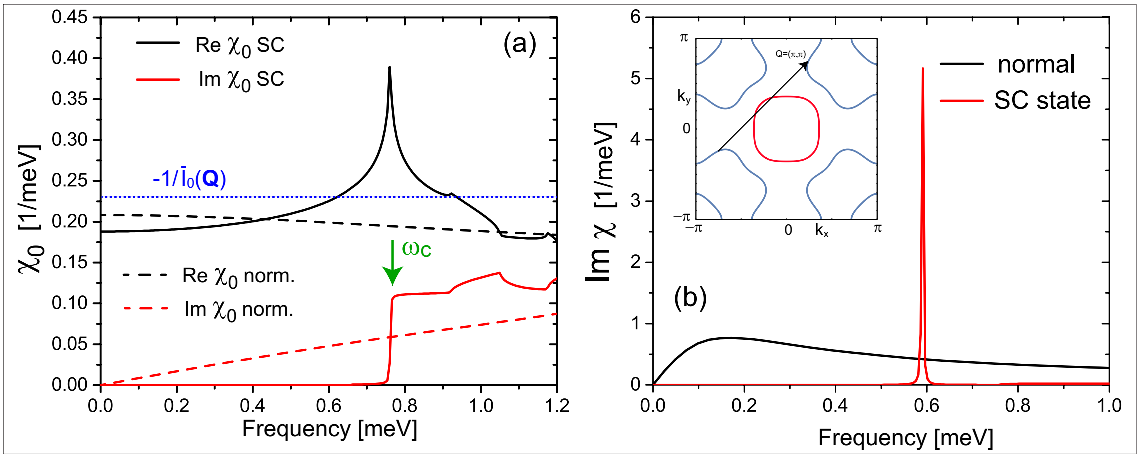

Supplementary Figure 6: χ in the spin-exciton scenario at $\mathbf{Q}_{\mathrm{AF}}$. (a) Real and imaginary parts of χ_0 at $\mathbf{Q}_{\mathrm{AF}}$ in the normal (dashed lines) and superconducting (solid lines) state of $\mathrm{CeCoIn_5}$. The onset energy ω_{c} of the particle-hole continuum in the superconducting state is shown by a green arrow. The blue dotted line indicates the value of $-1/\bar{I}_0(\mathbf{Q})$, such that its intersection with Re χ_0 in the superconducting state for $\omega < \omega_{\mathrm{c}}$ yields the position of the spin exciton. (b) Full χ in the normal and superconducting state at $\mathbf{Q}_{\mathrm{AF}}$. Inset: Fermi surface and scattering vector $\mathbf{Q}_{\mathrm{AF}}$ between momentum states on the Fermi surface.

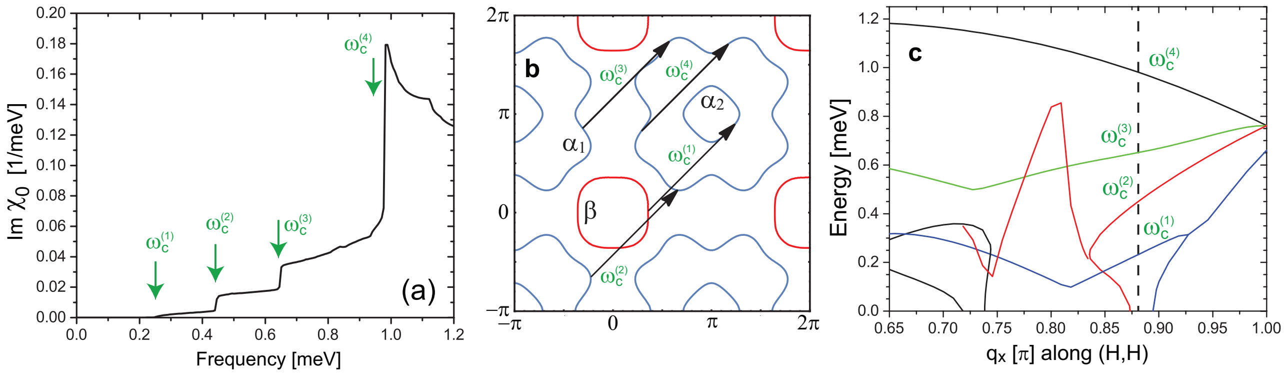

Supplementary Figure 7: χ in the spin-exciton scenario at $0.88\mathbf{Q}_{\mathrm{AF}}$. (a) Imaginary parts of χ_0 at $\mathbf{q} = 0.88\mathbf{Q}_{\mathrm{AF}}$ in the superconducting state of $\mathrm{CeCoIn_5}$. The onset energies $\omega_{\mathrm{c}}^{(i)}$ of the particle-hole continuum in the superconducting state are shown by green arrows. (b) Fermi surfaces in the extended Brillouin zone with scattering vectors corresponding to $\omega_{\mathrm{c}}^{(i)}$ in (a). (c) Momentum dependence of the onset energies $\omega_{\mathrm{c}}^{(i)}$ along the [1,1,0] direction. The dashed line corresponds to the momentum $\mathbf{q} = 0.88\mathbf{Q}_{\mathrm{AF}}$ for which Im χ_0 is shown in (a), with the indicated $\omega_{\mathrm{c}}^{(i)}$ being the same as in (a).

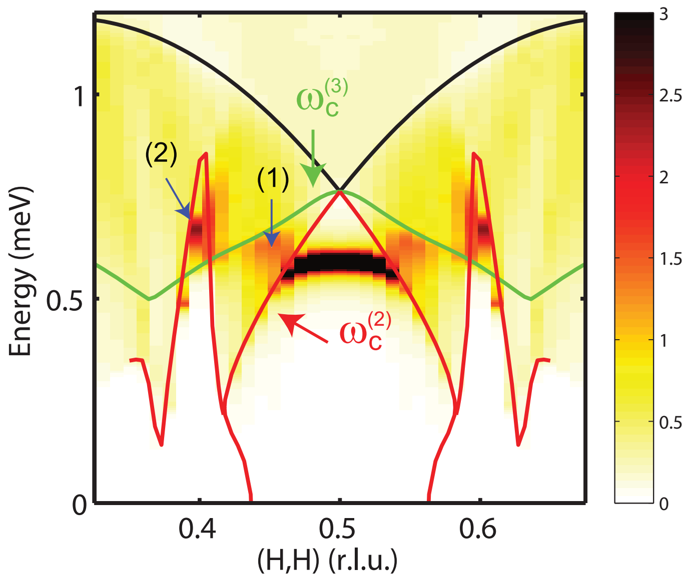

Supplementary Figure 8: Momentum dependence of the resonance as a spin-exciton with some of the onset energies of Fig. 7(c) overlain as solid lines.

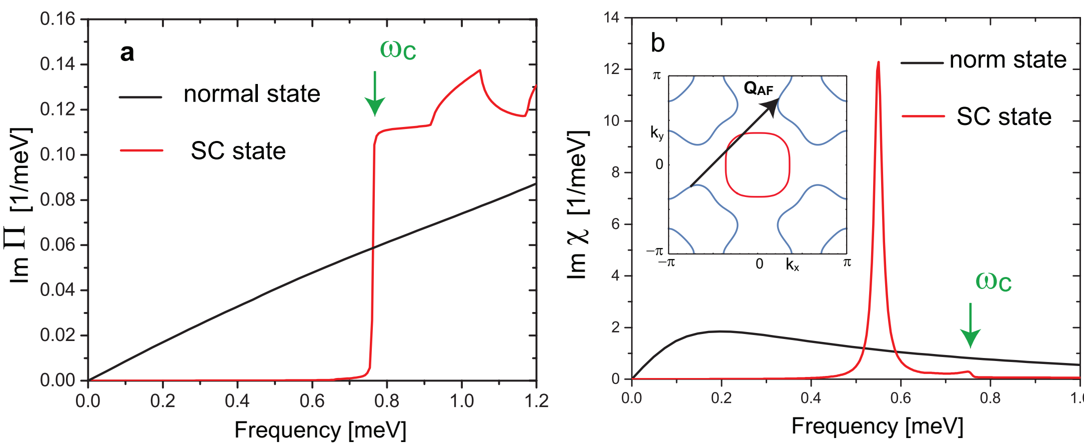

Supplementary Figure 9: The resonance as a magnon-like excitation at $\mathbf{Q}_{\mathrm{AF}}$. (a) Imaginary parts of Π at $\mathbf{Q}_{\mathrm{AF}}$ in the normal (black line) and superconducting (red line) state of $CeCoIn_5$. The onset energy ω_c of the particle-hole continuum in the superconducting state is shown by a green arrow. (b) Full χ in the normal (black line) and superconducting (red line) state $\mathbf{Q}_{\mathrm{AF}}$. The resonance occurs at $\omega = \Delta_{\mathrm{sw}}$ below ω_c (see green arrow). Inset: Scattering process contributing to Im Π.

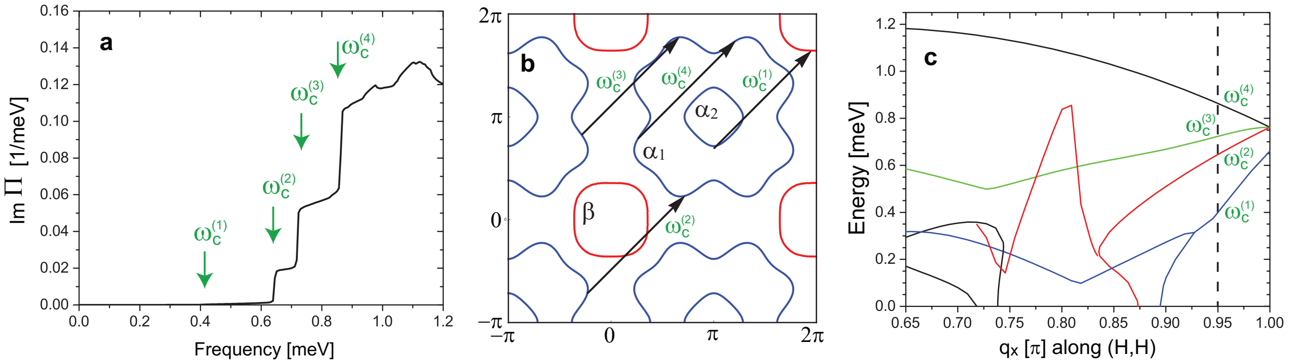

Supplementary Figure 10: The resonance as a magnon-like excitation at $0.95\mathbf{Q}_{\mathrm{AF}}$. (a) Imaginary part of Π in the superconducting state of $\mathrm{CeCoIn_5}$ at $\mathbf{q} = 0.95\mathbf{Q}_{\mathrm{AF}}$. The onset energies $\omega_c^{(i)}$ for particle-hole scattering in the superconducting state are shown by green arrows. (b) Fermi surfaces in the extended Brillouin zone with scattering vectors corresponding to $\omega_c^{(i)}$ in (a). (c) Momentum dependence of $\omega_c^{(i)}$ along $q_x = q_y$. The dashed line corresponds to the momentum $\mathbf{q} = 0.95\mathbf{Q}_{\mathrm{AF}}$ for which Im Π is shown in (a), with the indicated $\omega_c^{(i)}$ being the same as in (a).

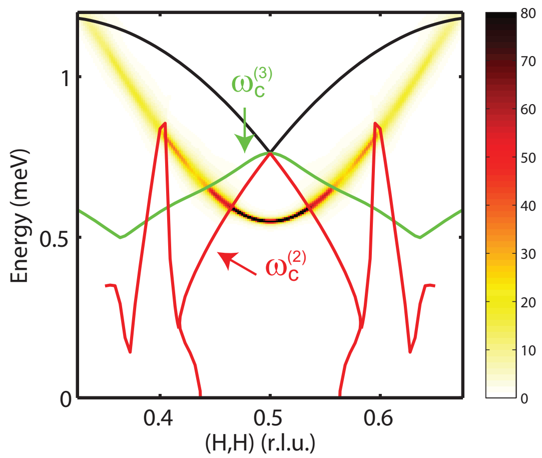

Supplementary Figure 11: Momentum dependence of the resonance as a magnon-like excitation with some the onset energies of SFig. 10(b) overlain as solid lines.

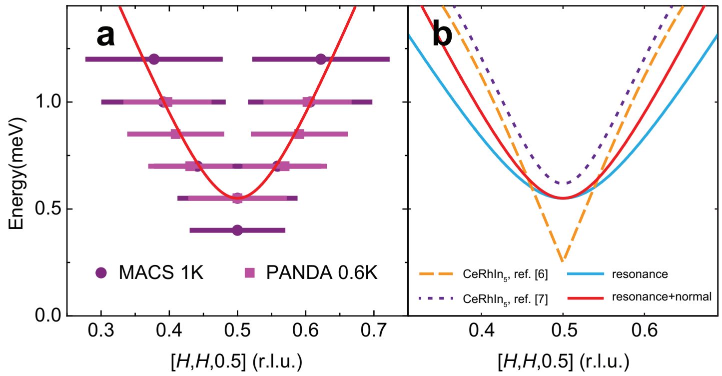

Supplementary Figure 12: Comparison of dispersive magnetic excitations in $Ce_{0.95}Yb_{0.05}CoIn_5$ with spin waves in $CeRhIn_5$. (a) Dispersion of magnetic excitations along $[H, H, 0.5]$ in $Ce_{0.95}Yb_{0.05}CoIn_5$ in the superconducting state obtained at 0.6 K on PANDA and 1 K on MACS. The points are obtained from scans in Figure 2(c) and Figure 3(c), (f), (i), (l) and (o). The solid red curve is the fit to $E = \sqrt{\Delta^2 + (c\mathbf{q})^2}$ with $\Delta = 0.55(1)$ meV and $c = 4.0(1)$ meV$\cdot$ Å. (b) Comparison of dispersion of magnetic excitations in $CeRhIn_5$ and $Ce_{0.95}Yb_{0.05}CoIn_5$, similar to Figure 1(j) but with the red curve from (a) also added in for comparison. The response in the superconducting state can be thought of as the sum of the resonance mode and normal state excitations and since the normal state response are broad peaks centered at $\mathbf{Q}_{\mathrm{AF}}$, the dispersion of the magnetic excitations in the superconducting state (resonance plus normal state excitations) has a larger velocity than the resonance itself.

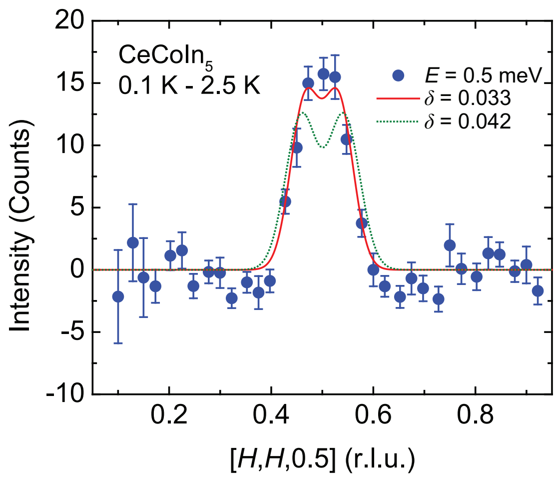

Supplementary Figure 13: Peak width of the resonance in $CeCoIn_5$ at $E = 0.5$ meV. Constant-energy scan along $[H, H, 0.5]$ centered at $\mathbf{Q}_{\mathrm{AF}}$ for $E = 0.50$ meV, obtained by subtracting 2.5 K data from 0.1 K data for $CeCoIn_5$. The cut is obtained by binning data with $0.42 < L < 0.58$. The data is fit with two Gaussian peaks separated by 2δ. The dashed green line shows the best fit by fixing $\delta = 0.042$, and the solid red line is the best fit by fixing $\delta = 0.033$.

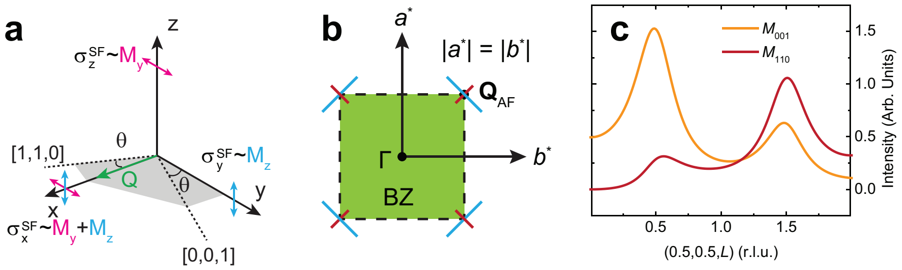

Supplementary Figure 14: Possible contribution to the resonance polarized along [1, 1, 0]. (a) Scattering geometry of polarized neutron scattering experiment used in previous work [4]. (b) Schematic of the reciprocal space for $CeCoIn_5$ with tetragonal symmetry. The green box indicate the first Brillouin zone, unlike Γ, anisotropy at $\mathbf{Q}_{\rm AF}$ = (0.5,0.5) between the longitudinal direction ([1, 1, 0], red solid line) and the tranverse direction ([1, $\bar{1}$, 0], blue solid line) does not break the four-fold rotational symmetry of the underlying lattice. (c) Comparison of M_{110} and M_{001} at $\mathbf{Q}_{\rm AF}$ = (0.5,0.5,0.5). In unpolarized neutron scattering measurements, M_{110} contributes little to the overall intensity near L = 0.5 but becomes significant near L = 1.5, where absorption becomes strong.

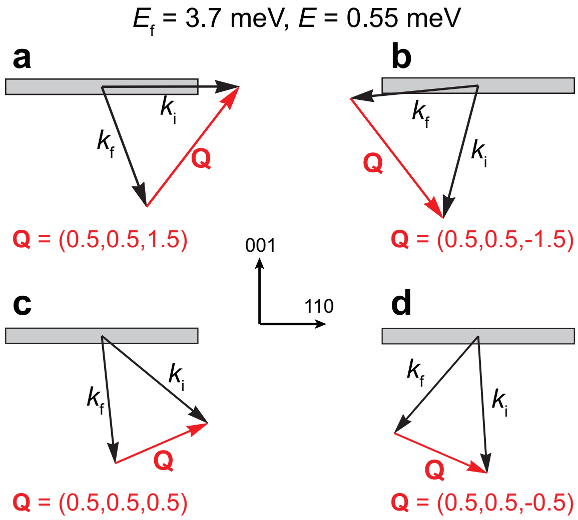

Supplementary Figure 15: Scattering geometries at several different wave vectors. (a) Scattering triangle for $\mathbf{Q}$ = (0.5,0.5,1.5) for $E_{\rm f}$ = 3.7 meV and E = 0.55 meV, the slab represents the sample array which is much longer along [1, 1, 0] than [0, 0, 1]. (b), (c) and (d) show similar scattering triangles for $\mathbf{Q}$ = (0.5,0.5,-1.5), (0.5,0.5,0.5) and (0.5,0.5,-0.5).

Supplementary Note 1: The Magnetic Resonance as a Spin Exciton

Within the spin-exciton scenario [5–14], a magnetic resonance emerges below T_c as a feedback effect of the unconventional superconducting order parameter on the spin excitation spectrum. This feedback effect can be easily understood by considering the full spin susceptibility in the random-phase approximation (RPA) which is given by [see Supplementary Eq. 42 in Ref.[15]]

$$\chi(\mathbf{q},\omega) = \frac{1}{2}\frac{\chi_0(\mathbf{q},\omega)}{1+\bar{I}_0(\mathbf{q})\chi_0(\mathbf{q},\omega)} \tag{S1}$$

where χ_0 is the non-interacting susceptibility and $\bar{I}_0(q)$ is the bare magnetic interaction, which was extracted in Ref. [15]. We employ Supplementary Eq. 39 in Ref.[15] to compute $\chi_0(\mathbf{q},\omega)$. To understand the emergence of a resonance, we begin by considering the form of χ_0 at $\mathbf{q} = \mathbf{Q}_{\rm AF}$ in the normal and superconducting states, as shown in Supplementary Fig. 6(a).

In the normal state, Imχ_0 increases linearly, while Reχ_0 is featureless and decreases monotonically. In contrast, in the superconducting state, Imχ_0 vanishes below an onset energy $\omega_c(\mathbf{Q}_{\rm AF})$ where it exhibits a sharp jump. Similar to the discussion in the magnon-like scenario below, the scattering of electrons from $\mathbf{k}$ to $\mathbf{k}+\mathbf{Q}_{\mathrm{AF}}$ requires the breaking of Cooper pairs and thus a minimum energy – the onset energy for non-zero $\mathrm{Im}\chi_0$ – given by $\omega_c(\mathbf{Q}_{\mathrm{AF}}) = |\Delta_{\mathbf{k}}|+|\Delta_{\mathbf{k}+\mathbf{Q}_{\mathrm{AF}}}|$. The corresponding scattering process is shown in the inset of Supplementary Fig. 6(b). As previously pointed out, the sharp jump of $\mathrm{Im}\chi_0$ at ω_{c} arises since the scattering process involves momentum states on the Fermi surface that possess opposite signs of the superconducting gap. As a result, $\mathrm{Re}\chi_0$ exhibits a logarithmic divergence at ω_{c} and the resonance condition $1 + \bar{I}_0(\mathbf{Q}_{\mathrm{AF}})\mathrm{Re}\chi_0(\mathbf{Q}_{\mathrm{AF}}, \omega_{\mathrm{R}}) = 0$ can be satisfied at a frequency $\omega_{\mathrm{R}} < \omega_{\mathrm{c}}$ for arbitrary small interaction $\bar{I}_0(\mathbf{Q}_{\mathrm{AF}})$, as follows from the intersection of $-1/\bar{I}_0(\mathbf{Q}_{\mathrm{AF}})$ and $\mathrm{Re}\chi_0$ shown in Supplementary Fig. 6(a). At the same time, $\mathrm{Im}\chi_0(\mathbf{Q}_{\mathrm{AF}}, \omega_{\mathrm{R}})$ vanishes as well (since $\omega_{\mathrm{R}} < \omega_{\mathrm{c}}$), giving rise to a sharp peak in $\mathrm{Im}\chi(\mathbf{Q}_{\mathrm{AF}}, \omega)$ at ω_{R}.

For momenta away from $\mathbf{Q}_{\mathrm{AF}}$, there exist multiple scattering channels for the same scattering vector $\mathbf{q}$ with different onset energies, $\omega_{\mathrm{c}}^{(i)}(\mathbf{q})$, as follows from a plot of $\mathrm{Im}\chi_0$ as a function of frequency at $\mathbf{q} = 0.88\mathbf{Q}_{\mathrm{AF}}$ in Supplementary Fig. 7(a). The scattering vectors corresponding to the various onsets are shown in Supplementary Fig. 7(b), while the momentum dependence of $\omega_{\mathrm{c}}^{(i)}(\mathbf{q})$ along the diagonal direction is shown in Supplementary Fig. 7(c).

According to the above discussion, no resonance can exist below $\omega_{\mathrm{c}}^{(1)}$, due to the absence of a logarithmic divergence associated with $\omega_{\mathrm{c}}^{(1)}$. This is confirmed by a plot of $\mathrm{Im}\chi$ together with the onset energies along the diagonal direction, shown in Supplementary Fig. 8. Moreover, as expected we find that in the vicinity of $\mathbf{Q}_{\mathrm{AF}}$, a resonance exists only below $\omega_{\mathrm{c}}^{(2)}$, due to the large value of $\mathrm{Im}\chi_0$ for $\omega > \omega_{\mathrm{c}}^{(2)}$. However, away from $\mathbf{Q}_{\mathrm{AF}}$, weaker resonances can exist even above $\omega_{\mathrm{c}}^{(2)}$ [see arrow (1)] or $\omega_{\mathrm{c}}^{(3)}$ [see arrow (2)] due to a smaller $\mathrm{Im}\chi_0$ at higher energies.

Supplementary Note 2: The Magnetic Resonance as an Undamped Paramagnon

The close proximity of superconductivity and the AF state in the cuprate superconductors had previously given rise to the suggestion that the magnetic resonance is a paramagnon that becomes undamped below T_c due to the opening of the particle-hole continuum. The suggestion that $\mathrm{CeCoIn_5}$ is close to an AF instability [16] raises the possibility that a similar scenario might be realized here. To explore this idea, we assume that the paramagnon dispersion is given by

$$\omega_{\mathrm{sw}}^2(\mathbf{q}) = \Delta_{\mathrm{sw}}^2 + c_{\mathrm{sw}}^2(\mathbf{q} - \mathbf{Q}_{\mathrm{AF}})^2 \tag{S2}$$

where Δ_{sw} is the spin-wave gap and c_{sw} is the spin-wave velocity. In the paramagnetic state, $\Delta_{\mathrm{sw}} = c_{\mathrm{sw}}/\xi$ where ξ is the magnetic correlation length. The presence of a magnetic anisotropy modifies Δ_{sw} and can lead to different values of Δ_{sw} for different spin polarizations. Above T_c, the paramagnon is strongly damped due to its coupling to particle-hole excitations. However, in the superconducting state, the mode can become undamped if Δ_{sw} is smaller than the onset energy for the particle hole continuum. The values of Δ_{sw} can be T_c and sample dependent. For example, La-doping to $\mathrm{CeCoIn_5}$ suppresses T_c and expands the lattice [17]. This process may bring $\mathrm{Ce_{1-x}La_xCoIn_5}$ closer to AF ordered phase with a reduced Δ_{sw} and T_c. Similarly, Yb-doped $\mathrm{CeCoIn_5}$ may also be closer to AF ordered phase with reduced T_c and Δ_{sw}.

To further explore this idea, we employ the spin-fermion scenario [18] where the spin-propagator is given by

$$\chi^{-1} = \bar{\chi}^{-1} - \Pi \tag{S3}$$

with $\bar{\chi}$ being the bare spin propagator and Π is the irreducible polarization operator. Since Re $\chi^{-1} = \bar{\chi}^{-1} - \mathrm{Re}\Pi$ is determined by electronic excitations at all energies, it cannot be computed within the current model. We therefore will use the phenomenological form

$$\mathrm{Re}\chi^{-1} = \bar{\chi}^{-1} - \mathrm{Re}\Pi = \frac{\omega_{\mathrm{sw}}^2(\mathbf{q}) - \omega^2}{\alpha} \tag{S4}$$

with the parameters in $\omega_{\mathrm{sw}}^2(\mathbf{q})$ being determined to correctly reproduce the dispersion of the experimentally observed resonance mode with $\Delta_{\mathrm{sw}} = 0.5498$ meV and $c_{\mathrm{sw}} = 3.2463$ Å^{-1}. Here, α reflects the (in general momentum dependent) spectral weight of the mode above T_c. We assume that the opening of the superconducting gap below T_c will not change the above form. Within this scenario, the main effect on the spin excitation spectrum in the superconducting state arises from $\mathrm{Im}\Pi$, which describes the damping of the spin excitations due to their decay into particle-hole excitations. To lowest order in the spin-fermion coupling g, the polarization operator is given by

$$\Pi = g^2\chi_0 \tag{S5}$$

where χ_0 is the bare susceptibility introduced in Supplementary Equation 39 of Ref. [15] (for the calculation of χ_0, we take the same parameters as in Ref. [15]), and g is the strength of the electronic coupling to the spin-wave mode. Below, we use for concreteness $g^2 = 20.0$ meV^2, however, we note that the specific value of g^2 does not affect the position of the resonance, only its width. In Supplementary Fig. 9(a) we plot ImΠ at $\mathbf{Q}_{\rm AF}$ both in the normal and superconducting state. While ImΠ increases linearly in the normal state, it vanishes below a certain onset energy, $\omega_{\rm c}$, in the superconducting state. This onset energy arises since the decay of the spin excitation into a particle-hole pair with momenta $\mathbf{k}$ and $\mathbf{k} + \mathbf{Q}_{\rm AF}$ (which both lie on the Fermi surface) requires a minimum energy given by $\omega_{\rm c}(\mathbf{Q}_{\rm AF}) = |\Delta_{\mathbf{k}}| + |\Delta_{\mathbf{k}+\mathbf{Q}_{\rm AF}}|$. The corresponding scattering process is shown in the inset of Supplementary Fig. 9(b). If $\Delta_{\rm sw} < \omega_{\rm c}(\mathbf{Q}_{\rm AF})$, the spin mode becomes undamped in the superconducting state, and Im χ exhibits a significant increase in intensity, as shown in Supplementary Fig. 9(b).

Away from $\mathbf{Q}_{\rm AF}$, several scattering channels with different onset energies emerge, as shown in Supplementary Fig. 10(a) where we plot ImΠ as a function of energy at $\mathbf{q} = 0.95\mathbf{Q}_{\rm AF}$. The lowest energy onset, $\omega_{\rm c}^{(1)}$, arises from a scattering channel that connects the α_2 and β Fermi surfaces as shown in Supplementary Fig. 10(b). Since this scattering channel connects momentum points $\mathbf{k}$ and $\mathbf{k} + \mathbf{q}$ on the Fermi surfaces that possess the same sign of the superconducting gap, ImΠ increases linearly in energy above $\omega_{\rm c}^{(1)}$, and does not exhibit a sharp jump. The three remaining higher energy onsets all connect momenta on the $\alpha_{1,2}$ Fermi surfaces, with opposite phase of the superconducting order parameter, hence leading to sharp jumps in Imχ_0 at the corresponding $\omega_{\rm c}^{(2-4)}$. The momentum dependence of these onset energies along the diagonal direction is shown in Supplementary Figs. 10(c). While the energy of the paramagnon lies always above $\omega_{\rm c}^{(1)}$, ImΠ is rather small for energies $\omega_{\rm c}^{(1)} < \omega < \omega_{\rm c}^{(2)}$, such that the paramagnon is only very weakly damped for energies $\omega < \omega_{\rm c}^{(2)}$, but becomes increasingly damped as its energy crosses $\omega_{\rm c}^{(2,3)}$.

To demonstrate this, we present in Supplementary Fig. 11 an intensity plot of Imχ as a function of frequency and momentum along the diagonal direction together with the onset energies, $\omega_{\rm c}^{(2,3)}$. Clearly, the intensity of the resonance mode decreases as its energy crosses $\omega_{\rm c}^{(2,3)}$.

Supplementary Note 3: Dispersion of the magnetic excitations in the superconducting state

In Figure 1(d)-(f), dispersion of the resonance mode is plotted for $\rm Ce_{0.95}Yb_{0.05}CoIn_5$ (as determined from the difference of the data well below and above T_c). In Supplementary Figure 12(a), the dispersion of the magnetic excitations in the superconducting state is plotted (as determined from the data well below T_c). Since the normal state magnetic excitations are broad peaks centered at $\mathbf{Q}_{\rm AF}$, the dispersion obtained after subtracting the normal state response disperses slower compared to the dispersion obtained from the superconducting state alone (sum of the resonance mode and the normal state response). By fitting the dispersion in Supplementary Figure 12(a) with $E = \sqrt{\Delta^2 + (c|\mathbf{q}|)^2}$ (solid red line), we find $\Delta = 0.55(1)$ meV and $c = 4.0(1)$ meV·Å compared to $\Delta = 0.55(1)$ meV and $c = 3.2(1)$ meV·Å in Figure 1(d)-(f). This value of c is closer to $c = 4.8(2)$ meV·Å [2] and $c \approx 5.2$ meV·Å [3] in $\rm CeRhIn_5$.

The magnon-like resonance mode in $\rm Ce_{0.95}Yb_{0.05}CoIn_5$ therefore is slightly softened compared to spin waves in $\rm CeRhIn_5$. This behavior is very different from the upward dispersing resonance found in iron pnictides, where the dispersion of the resonance [$c_{\rm res} = 50(5) - 85(5)$meV·Å] is much softer than the spin waves ($c \approx 450$ meV·Å) [19], this is not surprising considering the upward dispersing resonance in iron pnictides can be interpreted as a weak coupling spin-exciton. The comparison of dispersion for spin waves in $\rm CeRhIn_5$ and magnetic excitations in $\rm Ce_{0.95}Yb_{0.05}CoIn_5$ is shown Supplementary Figure 12(b), which is similar to Figure 1(j) but has the solid red line for the dispersion of the magnetic excitations in the superconducting state (resonance+normal) shown as well.

Supplementary Note 4: Incommensurate excitations at $E = 0.5$ meV

Recently, incommensurate spin excitations at $(0.5 \pm \delta, 0.5 \pm \delta, 0.5)$ were suggested in $\rm CeCoIn_5$ with δ=0.042(2) at $E = 0.5$ meV [4]. The incommensurate peaks were argued to be a dynamical precursor to the field-induced magnetically ordered Q phase just below H_{c2} [the Q phase orders at $(0.5 \pm \delta, 0.5 \pm \delta, 0.5)$ with δ=0.05(1)] [20]. We were unable to confirm the incommensurate excitations at $E = 0.5$ meV in $\rm CeCoIn_5$ from our experiment at MACS.

To understand how the poorer resolution in our experiments affect our ability to resolve possible incommensurate features, a cut along $[H, H, 0.5]$ at $E = 0.5$ meV is shown in Supplementary Figure 13 and fit with two Guassian peaks separated by 2δ for our data on $\rm CeCoIn_5$. While $\delta = 0.042$ does not provide a good fit to our results, a smaller splitting of $\delta = 0.033$ can describe our data. The smaller splitting of $\delta = 0.033$ from our data is inconsistent with δ=0.05(1) for the Q phase [20].

Moreover, our inelastic neutron scattering results on $Ce_{1-x}Yb_xCoIn_5$ suggests that the upwards dispersing excitations are ring-like [Fig. 5(c)-5(f)], emanating from $\mathbf{Q}_{\rm AF}$ rather than two peaks at $(0.5 \pm \delta, 0.5 \pm \delta, 0.5)$ as suggested in Ref. [4]. It is possible that there is more than a single contribution to the resonance, with the upward dispersing mode we observe being the dominant feature and an incommensurate mode exists around $E = 0.5$ meV. In this case, the smaller δ we observe comes from bottom of the upward dispersing mode at the commensurate wave vector at $E > 0.5$ meV, which mixes with the incommensurate mode at $E \approx 0.5$ meV due to our poorer resolution. More measurements with better energy and momentum resolutions are needed to clarify the fine details of the resonance around $E = 0.5$ meV. However, our data and analysis are fully consistent with the raw data in Ref. [4], both showing no downward dispersion of the resonance characteristic of a spin-exciton expected for a d-wave superconductor.

Supplementary Note 5: Anisotropy of spin excitations at $\mathbf{Q}_{\rm AF}$

In previous unpolarized and polarized neutron scattering experiments, it was concluded that the resonance spin excitations are exclusively polarized along the c-axis [1, 4]. Here we discuss the possibility of spin excitations polarized along the in-plane longitudinal direction [the [1,1,0] direction at $\mathbf{Q}_{\rm AF} = (0.5, 0.5, 0.5)$] in addition to the c-axis polarized excitations. It should be noted the such anisotropy does not break four fold rotational symmetry of $CeCoIn_5$ as required by the tetragonal crsytal structure, since we are distinguishing between the in-plane longitudinal and transverse directions [the [1,-1,0] direction at $\mathbf{Q}_{\rm AF} = (0.5, 0.5, 0.5)$] [Supplementary Figure 14(b)].

In previous polarized neutron scattering results [4], spin-flip (SF) neutron scattering cross sections $\sigma_x^{\rm SF}$, $\sigma_y^{\rm SF}$, and $\sigma_z^{\rm SF}$ as shown in Supplementary Figure 14(a) were measured where x indicates that neutron polarization direction is parallel to $\mathbf{Q}$, y is perpendicular to $\mathbf{Q}$ but within the scattering plane ($[H, H, L]$ plane), and z is perpendicular to the scattering plane. Since $\sigma_x^{\rm SF}$, $\sigma_y^{\rm SF}$, and $\sigma_z^{\rm SF}$ measures magnetic excitations perpendicular to both $\mathbf{Q}$ and the neutron polarization direction, $\sigma_x^{\rm SF} \propto M_y + M_z$, $\sigma_y^{\rm SF} \propto M_z$, and $\sigma_z^{\rm SF} \propto M_y$ [see Supplementary Figure 14(a)]. At $\mathbf{Q}_{\rm AF} = (0.5, 0.5, 0.5)$, M_y and M_z can be related to magnetic excitations along crystallographic axes by $M_y = M_{110} \sin^2\theta + M_{001}\cos^2\theta$ and $M_z = M_{1\bar{1}0}$, with θ being the angle between $\mathbf{Q}_{\rm AF}$ and $[1, 1, 0]$ [Supplementary Figure 14(a)]. Previous polarized neutron scattering measurements [4] conclusively demonstrated vanishing intensity of M_z compared to M_y, or $M_{1\bar{1}0} \approx 0$. It was then argued that due to tetragonal symmetry of $CeCoIn_5$, $M_{110} = M_{1\bar{1}0}$ and so only M_{001} is present [4]. However, this analysis did not make the distinction between the in-plane longitudinal and transverse directions that is allowed by four fold symmetry of the system, and the polarized experiment only ruled out the excitations polarized along the in-plane transverse direction. The presence of spin-orbit coupling can induce in-plane spin excitation anisotropy, as seen in the tetragonal phase of iron pnictides [21].

From L-dependence obtained in unpolarized neutron scattering measurements, it was also argued that there are only excitations polarized along the c-axis [1]. However M_{110} contributes little to the total intensity near $L = 0.5$, but becomes significant for $L = 1.5$ [Supplementary Figure 14(c)], where neutron absorption becomes extremely strong since either $k_{\rm i}$ or $k_{\rm f}$ will be close to $[1, 1, 0]$ [Supplementary Fig. 15(a) and (b)], which does not happen for $L = 0.5$ [Supplementary Figures 15(c) and (d)]. The scattering triangles are shown for these cases together with the sample (gray slabs) in Supplementary Figure 15. When $L = 0.5$, for both scattering geometries [Supplementary Figures 15(c) and (d)], both directions of $k_{\rm i}$ and $k_{\rm f}$ are far away from $[1, 1, 0]$. When $L = 1.5$, either $k_{\rm i}$ or $k_{\rm f}$ becomes close to $[1, 1, 0]$ resulting in the neutron beam having to transverse more of the sample resulting in much stronger absorption.

This means even if there is a significant M_{110} contribution, it would be very difficult to observe it in either previous [1] or our work. Given the many crystals required for inelastic neutron scattering experiments (Supplementary Fig. 1), it would be rather difficult to estimate accurately the neutron absorption cross section and determine the M_{110} component. In conclusion, while $M_{1\bar{1}0}$ has been eliminated by polarized neutron scattering results [4], the presence of M_{110} along with M_{001} has not been ruled out by current experimental results and its presence is important for understanding the splitting of the resonance mode under an applied magnetic field.

[1] Stock, C., Broholm, C., Hudis, J., Kang, H. J., and Petrovic, C., Spin resonance in the d-Wave superconductor $CeCoIn_5$, Phys. Rev. Lett. **100**, 087001 (2008).

[2] Das, P *et al.*, Magnitude of the magnetic exchange interaction in the heavy-Fermion antiferromagnet $CeRhIn_5$, Phys. Rev. Lett. **113**, 246404 (2014).

[3] Stock, C., Rodriguez-Rivera, J. A., Schmalzl, K., Rodriguez, E. E., Stunault, A., and Petrovic, C., Single to multiquasi-particle excitations in the itinerant helical magnet $CeRhIn_5$, Phys. Rev. Lett. **114**, 247005 (2015).
[4] Raymond, S. and Lapertot, G., Ising Incommensurate Spin Resonance of $CeCoIn_5$: A Dynamical Precursor of the Q Phase, Phys. Rev. Lett. **115**, 037001 (2015).
[5] Eremin, I., Morr, D.K., Chubukov A.V., Bennemann K.H., and Norman, M.R., Novel resonance mode in $d_{x^2-y^2}$-wave supercondutors. Phys. Rev. Lett. **94**, 147001 (2005).
[6] Fong, H.F. *et al.*, Phonon and magnetic neutron scattering at 41 meV in $YBa_2Cu_3O_7$. Phys. Rev. Lett. **75**, 316-319 (1995).
[7] Abanov Ar. and Chubukov A.V., A relation between the resonance neutron peak and ARPES data in cuprates. Phys. Rev. Lett. **83**, 1652-1655 (1999).
[8] Brinckmann, J. and Lee, P.A., Slave boson approach to neutron scattering in $YBa_2Cu_3O_{6+y}$ superconductors. Phys. Rev. Lett. **82**, 2915-2918 (1999).
[9] Kao Y.-J., Si Q., and Levin, K., Frequency evolution of neutron peaks below T_c: Commensurate and incommensurate structure in $La_{0.85}Sr_{0.15}CuO_4$ and $YBa_2Cu_3O_{6.6}$. Phys. Rev. B **61**, R11898(R) (2000).
[10] Onufrieva, F. and Pfeuty, P., Spin dynamics of a two-dimensional metal in a superconducting state: Application to the high-T_c cuprates. Phys. Rev. B **65**, 054515 (2002).
[11] Manske D., Eremin, I., and Bennemann, K.H., Analysis of the resonance peak and magnetic coherence seen in inelastic neutron scattering of cuprate superconductors: A consistent picture with tunneling and conductivity data. Phys. Rev. B **63**, 054517 (2001).
[12] Norman, M.R., Relation of neutron incommensurability to electronic structure in high-temperature superconductors. Phys. Rev. B **61**, 14751 (2000).
[13] Norman, M.R., Magnetic collective mode dispersion in high-temperature superconductors. Phys. Rev. B **63**, 092509 (2001).
[14] Chubukov, A., Janko, B., and Tchernyshov, O., Dispersion of the neutron resonance in cuprate superconductors. Phys. Rev. B **63**, 180507(R) (2001).
[15] Van Dyke, J., Massee, F., Allan, M. P., Davis, J. C., Petrovic, C., and Morr, D. K., Direct evidence for a magnetic f-electron-mediated pairing mechanism of heavy-fermion superconductivity in $CeCoIn_5$, PNAS **111**, 11663-11667 (2014).
[16] Bianchi, A., Movshovich, R., Vekhter, I., Pagliuso, P. G. and Sarrao, J. L. Avoided antiferromagnetic order and quantum critical point in $CeCoIn_5$, Phys. Rev. Lett. **91**, 257001 (2003).
[17] Petrovic, C., Bud'ko, S. L., Kogan, V. G., and Canfield, P. C., Effects of La substitution on the superconducting state of $CeCoIn_5$, Phys. Rev. B **66**, 054534 (2002).
[18] Morr, D.K. and Pines, D., The resonance peak in cuprate supercondutors. Phys. Rev. Lett. **81**, 1086-1089 (1998).
[19] Kim, M. G. *et al.*, Magnonlike dispersion of spin resonance in Ni-doped $BaFe_2As_2$, Phys. Rev. Lett. **110**, 177002 (2013).
[20] Kenzelmann, M. *et al.*, Evidence for a Magnetically Driven Superconductivity Q Phase of $CeCoIn_5$, Phys. Rev. Lett. **104**, 127001 (2010).
[21] Luo , H. et al., Spin Excitation Anisotropy as a Probe of Orbital Ordering in the Paramagnetic Tetragonal Phase of Superconducting $BaFe_{1.904}Ni_{0.096}As_2$, Phys. Rev. Lett. **111**, 107006 (2013).